Stable sulfur isotope measurements to trace the fate of SO_2 in the Athabasca oil sands region

Neda Amiri[1], Roghayeh Ghahremaninezhad[2], Ofelia Rempillo[3], Travis W. Tokarek[4], Charles A. Odame-Ankrah[4,a], Hans D. Osthoff[4], and Ann-Lise Norman[1]

[1]Department of Physics and Astronomy, University of Calgary, Calgary, Canada
[2]Environment and Climate Change Canada, Toronto, Canada
[3]Physics Department, De La Salle University, Manila, Philippines
[4]Department of Chemistry, University of Calgary, Calgary, Canada
[a]now at: Global Analyzer Systems Ltd., Calgary

Correspondence to: Ann-Lise Norman (alnorman@ucalgary.ca)

Abstract. Concentrations and $\delta^{34}S$ values for SO_2 and size segregated sulfate aerosols were determined for Air Monitoring Station 13 (AMS13) at Fort MacKay in the Athabasca oil sands region, northeastern Alberta, Canada as part of the Joint Canada-Alberta Implementation Plan for Oil Sands Monitoring (JOSM) campaign from Aug 13 to Sep 5, 2013. Sulfate aerosols and SO_2 were collected on filters using a high-volume sampler, with 12 or 24 hour time intervals.

Sulfur dioxide (SO_2) enriched in ^{34}S was exhausted by a Chemical Ionization Mass Spectrometer (CIMS) operated at the measurement site and affected isotope samples for a portion of the sampling period. It was realized that this could be a useful tracer and samples collected were divided into two sets. The first set includes periods when the CIMS was not running (CIMS-OFF) and no $^{34}SO_2$ was emitted. The second set is for periods when the CIMS was running (CIMS-ON) and $^{34}SO_2$ was expected to affect SO_2 and sulfate high-volume filter samples.

$\delta^{34}S$ values for sulfate aerosols with D>0.49 μm during CIMS-OFF periods (no tracer $^{34}SO_2$ present) indicate the sulfur isotope characteristics of secondary sulfate in the region. Such aerosols had $\delta^{34}S$ values that were isotopically lighter (down to -4.5 ‰) than what was expected according to potential sulfur sources in the Athabasca oil sands region (+3.9 ‰ to +11.5‰). Lighter $\delta^{34}S$ values for larger aerosol size fractions is contrary to expectations for a primary unrefined sulfur from untreated oil sands (+6.4 ‰) mixed with secondary sulfate from SO_2 oxidation and accompanied by isotope fractionation in gas phase reactions with OH, or the aqueous phase by H_2O_2 or O_3. Significant anti-correlations between $\delta^{34}S$ values of dominantly secondary sulfate aerosols with D<0.49 μm and the concentrations of Fe and Mn (r = -0.80 and r = -0.76, respectively) were observed. These results indicate that SO_2 was oxidized by a transition metal ion (TMI) catalyzed pathway involving O_2 and Fe^{3+} and/or Mn^{2+}, an oxidation pathway known to favor lighter sulfur isotopes.

Analysis of ^{34}S enhancements of sulfate and SO_2 during CIMS-ON periods indicated rapid oxidation of SO_2 from this local source at ground level on the surface of aerosols before reaching the high-volume sampler or on the collected aerosols on the filters in the high-volume sampler.

Correlations between SO_2 to sulfate conversion ratio (F(s)) and the concentrations of α-pinene (r = 0.85), β-pinene (r = 0.87), and limonene (r = 0.82) during daytime indicate that SO_2 oxidation by Criegee biradicals may be a potential oxidation pathway

in highly polluted regions.

1 Introduction

Sulfate aerosols are known to impact ecosystems and climate through their deposition and radiative effects. The deposition of sulfate aerosols can cause acidification of soils and lakes (Gerhardsson, 1994). Furthermore, their direct and indirect radiative effects can change the radiative budget at regional scales and alter climate (IPCC, 2001).

Sulfate aerosols can be primary or secondary. Primary particles are emitted directly from the surface to the atmosphere but secondary particles are formed in the atmosphere through gas to particle conversion. The majority of anthropogenic and natural sulfur is emitted as sulfur dioxide (SO_2) or oxidized to SO_2 in the atmosphere (Berresheim et al., 1995; Berresheim, 2002; Seinfeld and Pandis, 1998). Chin and Jacob (1996) and Chin et al. (2000) estimated that around 50% of the globally emitted SO_2 is oxidized to form sulfate and the remainder is lost by dry and wet deposition.

Dry deposition is important and gives SO_2 a lifetime of about 3 days for a boundary layer with 1000 m depth (Hicks, 2006; Myles et al., 2007). Wet deposition is important intermittently for rainy days or days with fog. The lifetime of SO_2 in the atmosphere can vary greatly from hours to days depending on measurement location, season, time of day, etc. As an example, Hains (2007) measured SO_2 lifetime in the eastern US and found values of 19 ± 7 h. GEOS-Chem simulations suggest a value of 13 h during summer for the same location.

A detailed understanding of SO_2 oxidation pathways and their relative importance is critical for accurate representation of sulfate's spatial distribution as well as its impact on climate through aerosol radiative forcing.

The oil sands regions are of great interest because of the large quantities of SO_2 emissions (Fioletov et al., 2016; McLinden et al., 2012; Percy, 2013). Therefore, a comprehensive knowledge of SO_2 oxidation pathways important in this region is useful to identify where and how atmospheric sulfur species are transported and contribute to aerosol formation, growth and acid deposition.

Oil sands extraction and upgrading processes can be a source of sulfate aerosols, SO_2 and oxidants. The major sources of SO_2 emissions in the Athabasca oil sands region are upgrading and energy production operations (Kindzierski and Ranganathan, 2006). Simpson et al. (2010) observed SO_2 enhancements over the oil sands region with a maximum value of 39 parts-per-billion by volume (10^{-9}, ppb) relative to a background value of 102 parts-per-trillion by volume (10^{-12}, ppt). Howell et al. (2014) showed that both SO_2 and sulfate contributions from the Athabasca oil sands region are significant compared to estimates for potential background sources of sulfur such as annual forest fire emissions in Canada. Bardouki et al. (2003) by the use of positive matrix factorization (PMF) modeling suggested that secondary sulfate is the second most important contributor to $PM_{2.5}$ mass in Fort MacKay (31%).

Sulfur dioxide (SO_2) is converted to sulfate in homogeneous and heterogeneous reactions. The oxidation pathway is a very important factor to determine the effects of the sulfate formed on the environment. Gas phase oxidation of SO_2 by hydroxyl radicals (OH) produces sulfuric acid (H_2SO_4) gas, which can nucleate in the atmosphere to form new particles (Tanaka et al.,

1994; Kulmala et al., 2004). These newly formed aerosol particles are buoyant and can be dispersed far from the emission source. Newly formed sulfate aerosols also impact direct radiative forcing by scattering sunlight back to space. These particles can grow by the addition of organics to create a large number of accumulation mode aerosols which are more easily deposited on local surfaces, increasing the potential for acidification at regional to local scales. They also have the ability to form cloud condensation nuclei (CCN) (Kulmala et al., 2004, 2007; Benson et al., 2008). After forming CCN they can increase the albedo and lifetime of clouds (Twomey, 1991; Boucher and Lohmann, 1995). Homogeneous oxidation of SO_2 in the gas phase by OH is as follows (Burkholder et al., 2015);

$$SO_2 + OH + M \rightarrow HOSO_2 + M \quad \text{(R1)}$$

$$HOSO_2 + O_2 \rightarrow HO_2 + SO_3 \quad \text{(R2)}$$

$$SO_3 + H_2O + M \rightarrow H_2SO_4 + M \quad \text{(R3)}$$

Seventeen to 36 $\%$ of global sulfate production can be attributed to this pathway (Chin et al., 2000; Sofen et al., 2011; Berglen, 2004).

Heterogeneous oxidation of SO_2 primarily occurs in cloud droplets, although oxidation on the surface of aerosols can be important regionally (Chin and Jacob, 1996). Heterogeneous oxidation prevents H_2SO_4 gas production and new particle formation. Sulfate formed by this pathway can modify the aerosol size distribution, which affects both direct and indirect aerosol forcing. Scattering efficiency of the particle population can be increased which is responsible for direct scattering (Hegg et al., 2004; Yuskiewicz et al., 1999). In addition, acidity of aerosols as well as their CCN activity of the particle population can be modified and affect the indirect radiative forcing (Mertes et al., 2005a, b). Eriksen et al. (1972) showed various steps in SO_2 dissolution before oxidation by major oxidants which are H_2O_2, O_3, and O_2 catalyzed by transition metal ions (TMIs) such as Fe^{3+} or Mn^{2+} in a radical chain reaction pathway (Herrmann et al., 2000).

$$SO_2(g) \rightleftharpoons SO_2(aq) \quad \text{(R4)}$$

$$SO_2(aq) + H_2O \rightleftharpoons HSO_3^- + H^+ \quad \text{(R5)}$$

$$HSO_3^- + H^+ \rightleftharpoons H_2SO_3 \quad \text{(R6)}$$

$$HSO_3^- \rightleftharpoons SO_3^{2-} + H^+ \quad \text{(R7)}$$

$$2HSO_3^- \rightleftharpoons H_2O + S_2O_5^{2-} \quad \text{(R8)}$$

After the dissolution, S(IV) is oxidized to S(VI) by O_3, H_2O_2, and O_2 in the presence of TMIs. The oxidation of SO_2 by O_3 and O_2 catalyzed by TMIs is pH dependent and becomes faster as pH increases, whereas oxidation by H_2O_2 within normal atmospheric pH ranges (2-7) does not depend on pH (Seinfeld and Pandis, 1998).

Field studies suggested that TMI-catalyzed oxidation is the dominant sulfate formation pathway in polluted environments in winter (Jacob et al., 1984, 1989; Jacob and Hoffmann, 1983). Oxygen isotope measurements of sulfate aerosols collected at Alert, Canada (82.5°N, 62.3°W) showed that TMI-catalyzed SO_2 oxidation is significant during winter (McCabe et al., 2006). Recent studies have shown that the TMI-catalyzed oxidation pathway is underestimated (more than an order of magnitude) in all current atmospheric chemistry models (Harris et al., 2013a, b). For example Harris et al. (2013a) measured the sulfur isotopic composition of SO_2 upwind and downwind of clouds and used the difference to calculate the fractionation that occurred for in-cloud SO_2 oxidation. They showed that SO_2 oxidation catalyzed by natural TMIs on mineral dust is the dominant in-cloud oxidation pathway and is underestimated by more than an order of magnitude in current atmospheric models. To the best of our knowledge there is no study to investigate the importance of the TMI-catalyzed pathway in SO_2 oxidation on the surface of aerosols in highly polluted areas such as the Alberta oil sands region during summer.

Until recently, OH radical initiated oxidation of SO_2 was considered the only gas phase oxidation pathway important in the atmosphere. However, recent measurements of the rate constants for oxidation of SO_2 by Criegee biradicals and model simulations of field observations have shown this pathway is more significant than previously thought (Berndt et al., 2012; Boy et al., 2013; Mauldin III et al., 2012; Sipilä et al., 2014). Criegee biradicals are formed through ozonolysis of unsaturated hydrocarbons such as biogenic terpenes (Boy et al., 2013; Welz et al., 2012). The rate constants of the reaction of Criegee biradicals and SO_2 are somewhat uncertain but researchers agree that the reaction is faster than what has been previously thought (e.g. 6×10^{-13} $cm^3molecule^{-1}s^{-1}$ and 8×10^{-13} $cm^3molecule^{-1}s^{-1}$ for Criegee biradicals originating from the ozonolysis of α-pinene and limonene, respectively (Mauldin III et al., 2012)). Several studies have linked biogenic volatile organic compound (BVOC) environments to an increase in SO_2 to sulfuric acid/sulfate conversion rates. For example, Mauldin III et al. (2012) reported the oxidation of SO_2 by Criegee biradicals faster than what has been thought before, during a field study in a boreal forest and confirmed the results by laboratory and theoretical studies.

In this study, we investigated the importance of the various SO_2 oxidation pathways, including Criegee biradicals in a polluted region with high VOC emissions using measurements of sulfates and SO_2 concentrations and isotopic composition.

Sulfur isotope analysis is a powerful tool to investigate SO_2 oxidation pathways in the atmosphere. As an example, Lin et al. (2017) used high sensitivity measurements of cosmogenic ^{35}S in SO_2 and sulfate from the ambient boundary layer over coastal California and Tibetan plateau to identify oxidation of SO_2 to sulfate. The lifetime in summer ranged from 1 to 2 days suggesting that there might be oxidation pathways which are more important than previously thought.

In this study, stable sulfur isotope values for SO_2 and size segregated sulfate aerosols were measured. $\delta^{34}S$ values of potential sources in the region (Proemse et al., 2012a) and isotope fractionation data (Harris et al., 2012) were used to investigate the

importance of atmospheric sulfur oxidation pathways in the Athabasca oil sands region. Sulfur dioxide (SO_2) to sulfate conversion ratio ($F(s) = \frac{[SO_4]}{[SO_4]+[SO_2]}$) was also used as a tool to investigate the possible SO_2 oxidants in the region. Although the data represent a short period of time and do not reflect the variability on a seasonal scale, Soares et al. (2018) showed that short term measurements are more suitable for source identification. He mentioned that the source signals of NO_2 and SO_2 emissions are available in hourly to daily time scales and long-term observation may cause a loss in short term variation.

2 Study site

Sulfate aerosols and SO_2 measurements were made at a monitoring site next to the Wood Buffalo Environmental Association's (WBEA) Air Monitoring Station 13 (AMS13) site just south of Fort MacKay in the Athabasca oil sands region from August 13 to September 5, 2013 as part of the Joint Canada-Alberta Implementation Plan for Oil Sands Monitoring (JOSM) project (Liggio et al., 2016; Phillips-Smith et al., 2017). The location of AMS13 is shown in Figure 1.

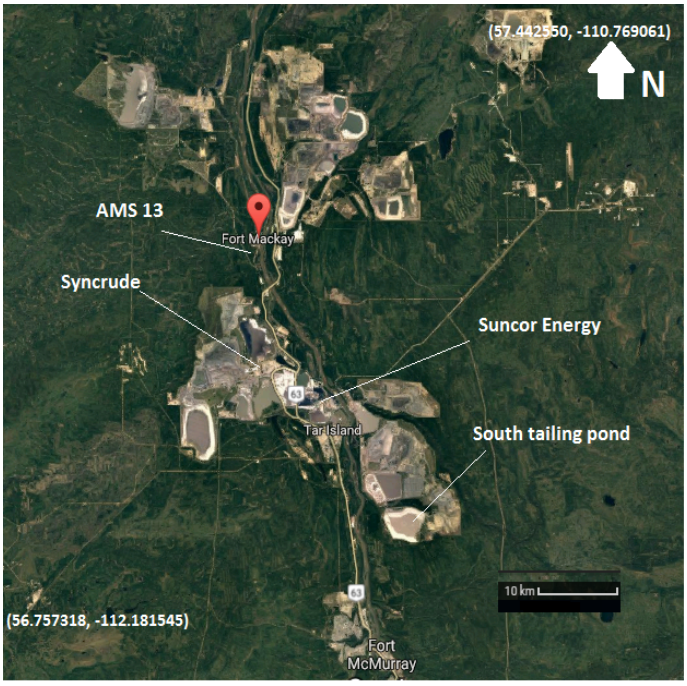

Figure 1. Wood Buffalo Air Monitoring Station 13 (AMS13) site, south of Fort MacKay (Map data ©2018 Google)

3 Sulfur isotopes

Stable sulfur isotopes can be used to investigate sulfur sources, transport and chemistry such as the relative importance of oxidation pathways (Puig et al., 2008; Krouse and Grinenko, 1991). Sulfur has four stable isotopes:^{32}S,^{33}S,^{34}S, and ^{36}S with

relative abundances of ∼95%, 0.75%, 4.21% and 0.015%, respectively. The isotopic composition is described using the delta notation:

$$\delta^x S(‰) = \left(\frac{\left(\frac{n(^xS)}{n(^{32}S)}\right)_{Sample}}{\left(\frac{n(^xS)}{n(^{32}S)}\right)_{V-CDT}} - 1\right) \times 1000 \quad (1)$$

where n is the number of atoms,^{x}S is the heavy isotope and V-CDT is the international sulfur isotope standard, Vienna Canyon Diablo Troilite, with the isotopic ratio of $R^{34} = \frac{^{34}S}{^{32}S} = 0.044163$, $R^{33} = \frac{^{33}S}{^{32}S} = 0.007877$ (Ding et al., 2001) and $R^{36} = \frac{^{36}S}{^{32}S} = 1.05 \times 10^{-4}$. For the purpose of this paper we only analyze $\delta^{34}S$ values and use $\delta^{33}S$ values to find enrichment of samples.

The isotopic composition ($\delta^{34}S$) of major sources of atmospheric sulfur in the Athabasca oil sands region were quantified by Proemse et al. (2012a). They reported sulfur isotope values for bitumen, +4.3±0.3 ‰, untreated oil sands, +6.4 ± 0.5 ‰ and the isotopic composition of products such as $(NH_4)_2SO_4$ which is produced in flue gas desulfurization (FGD), +7.2 ‰, coke, +4.0 ± 0.2 ‰ and elemental sulfur, +5.3 ± 0.5 ‰. Primary sulfate with diameter (D)<2.5 μm are reported to have $\delta^{34}S$ values between +7.0 ‰ to +7.8 ‰ with an average of +7.3 ± 0.3 ‰, and between +6.1 ‰ to +11.5 ‰ with an average of +9.4 ± 2 ‰ for two of the largest stacks in the region. These two stacks are 12.2 km and 19.4 km south and south east of the measuring site, respectively.

In addition to sulfur emissions from oil sands processing, aerosols can potentially be produced from vehicle exhaust. Combustion emissions from vehicles showed a $\delta^{34}S$ of +5 ‰ for SO_2 from engine exhaust in Alberta and British Columbia (Norman et al., 2004; Norman, 2004). On average, Diesel and gasoline contained very low amounts of sulfur (0.008%, (Norman, 2004)) and combustion produces both primary sulfate as well as SO_2. Other sulfur emissions in the region may result from anoxic conditions in the environment or the tailing ponds associated with sulfate reducing bacteria. Biogenic emissions of Hydrogen sulfide (H_2S) have negative $\delta^{34}S$ values which can be as negative as -30 ‰ (Wadleigh and Blake, 1999). H_2S is oxidized to SO_2 with a lifetime of 1 day (Brimblecombe et al., 1989) and the sulfur isotopic composition is not expected to change during oxidation of H_2S to SO_2 (Sanusi et al., 2006; Newman et al., 1991).

Differing isotopic contributions from sulfur sources can drive variations in aerosol sulfate $\delta^{34}S$ values. Another reason for $\delta^{34}S$ variation can be isotopic fractionation. The oxidation of SO_2 causes isotope fractionation between the products and reactants as long as the reaction is not complete. When the reactant is available as an infinite reservoir the fractionation factor is calculated as

$$\alpha_{34} = \frac{R_{Products}}{R_{Reactants}} \quad (2)$$

where $R = \frac{^{34}S}{^{32}S}$. Following the definition for α used by Harris et al. (2012) for both kinetic and equilibrium reactions, $\alpha < 1$ means that the light isotopes react faster, so products are isotopically lighter than the reactant.

During this study, minute quantities of $^{34}SO_2$ was emitted from a Chemical Ionization Mass Spectrometer (CIMS) exhaust 50 m away from the high-volume sampler near the ground for special periods. Here we refer to these particular periods as CIMS-

ON. The enrichment of $^{34}SO_2$ was sufficiently large that isotopic fractionation can be neglected during CIMS-ON periods. However, sulfur sources and oxidation pathways can be examined using $\delta^{34}S$ values for the periods when CIMS was not operational (CIMS-OFF). During SO_2 oxidation to sulfate, isotope fractionation occurs between reactants and products which is unique for each oxidation pathway. Note though sulfur isotope fractionation resulting from oxidation by Criegee biradicals is not currently known. Harris et al. (2012) reported temperature dependent fractionation factors for different SO_2 oxidation pathways as follows: sulfur dioxide (SO_2) oxidation by OH radicals favors heavy isotopes and the fractionation decreases slightly with temperature (equation 3).

$$(\alpha - 1)(‰) = (10.60 \pm 0.73) - (0.004 \pm 0.015) \times T(°C) \tag{3}$$

Aqueous phase oxidation can occur by H_2O_2 and O_3, fractionation during this pathway (equation 4) also prefers heavy isotopes and decreases with temperature slightly.

$$(\alpha - 1)(‰) = (16.51 \pm 0.15) - (0.085 \pm 0.004) \times T(°C). \tag{4}$$

The fractionation during TMI-catalyzed oxidation pathway acts in the opposite direction to the other two pathways. TMI-catalysis is the only known oxidation pathway which favors lighter isotopes in the product sulfate and the fractionation strongly depends on temperature (equation 5).

$$(\alpha - 1)(‰) = (-5.039 \pm 0.044) - (0.237 \pm 0.004) \times T(°C). \tag{5}$$

4 Methods

4.1 Field measurements

Temperature, relative humidity, wind speed and direction time series are shown in Figure A1. A diurnal cycle in RH is evident for all days during the campaign except August 25 which was a rainy period.

A high-volume sampler placed at ground level with a flow rate of $0.99 \pm 0.05\ m^3/min$ was used to collect aerosols and SO_2. The high-volume sampler was fitted with a five stage cascade impactor to collect size-segregated aerosols on glass fiber filters in five ranges of aerodynamic diameter as A (>7.2 μm), B (3.0-7.2 μm), C (1.5-3.0 μm), D (0.95-1.5 μm), and E (0.49-0.95 μm). The final filter for fraction $F_{<0.49\mu m}$ was a 20.3×25.4 cm glass filter to collect aerosols with D<0.49 μm. An SO_2 filter pretreated with potassium carbonate (K_2CO_3) and glycerol solution was located beneath these 6 size segregated aerosol filters (Norman, 2004). The sampling interval was 12 hours (daytime (05:00 to 17:00) and nighttime (17:00 to 5:00 next day)) for the first twelve days except August 20 and 27 after which samples were collected for 24 hours (05:00 to 05:00). Field blanks were collected on three separate occasions at the start, in the middle and at the end of the campaign. Filter blanks from the field were loaded and then unloaded, stored and analyzed using the same protocols as samples. The high-volume sampler was turned off during field blank sampling. Filters were stored in zip lock bags and kept in < 4°C and transferred to the lab for analysis.

WBEA SO_2 data was used with a sampling interval of five minutes. Ozone and NO_2 mixing ratios were measured by UV

absorption using a Thermo 49i O_3 monitor every 10 s and a blue diode laser cavity ring-down spectrometer every 1 s (data were averaged to 1 min) (Odame-Ankrah, 2015; Paul and Osthoff, 2010), respectively. The slope uncertainties of these measurements were $\pm 1\%$ and $\pm 10\%$, respectively. Radiometer measurements using a pair of spectral radiometers (one facing the zenith, the other the nadir direction) were used to determine actinic flux and to calculate photolysis frequencies (j values) (Osthoff et al., 2017). Iron (Fe) and Manganese (Mn) were measured by semi-continuous X-Ray Fluorescence (XRF) measurements of metals taken every hour on a filter tape with a measurement uncertainty of $\pm$ 10% (Phillips-Smith et al., 2017).

Monoterpenes were measured hourly by gas chromatography-ion trap mass spectrometry (GC-IT-MS) (Tokarek et al., 2017). Volatile Organic Compounds (VOCs), $C_2 - C_{12}$ were sampled in canisters over a period spanning 9:30 to 8:30 of the next day, and analyzed using gas chromatography mass spectrometery (GCMS). Detection limits for VOC measurements can be found in the online JOSM database (ftp://ftp.tor.ec.gc.ca/OS/AMS13).

A Chemical Ionization Mass Spectrometer (CIMS) similar to the one described by Sjostedt et al. (2007) was used to measure OH reactivity at a distance of 10 m horizontally from the high-volume sampler. Enriched $^{34}SO_2$ was emitted from an exhaust pipe at ground level <50 m to the east in an unused area containing shrubs. Enriched $^{34}SO_2$ affected a portion of our samples during CIMS-ON periods; these periods were used to trace the fate of local $^{34}SO_2$ emitted from the CIMS exhaust near the ground.

4.2 Analysis of high-volume filter samples

Filter papers were shredded and sonicated for 30 minutes in distilled deionized water in the laboratory (200 ml for SO_2 filters and filters to collect particles in size range $F_{<0.49\mu m}$ and 75 ml for slotted filters to collect particles in sizes larger than 0.49 μm). For SO_2 filters 1 ml of 30% w/w hydrogen peroxide (BDH) was added to oxidize the SO_2 to sulfate before sonication. Filter paper fibers were removed by 0.45 mm Millipore filtration, and 10 ml of the filtrate samples was analyzed using a Dionex ICS-1000 ion chromatography (IC) system with a Dionex IonPac AS14 column and electric conductivity detector to determine the concentration of sulfate with an uncertainty of 5%. Prior to treatment, the pH of the remaining filtrate was measured and found to be $\sim$6.0. The remaining filtrate was treated with 0.5 ml of 10% $BaCl_2$ (Dihydrate 99% (EMD)), and dilute (0.5 N) OmniTrace HCl (34-37% (EMD)) was added to samples until a pH of 3 was achieved. Approximately 100 μl of 0.5 N HCl was used for aerosol filters. The samples were then heated to facilitate precipitation of $BaSO_4$. Barium sulfate was isolated by Millipore filtration, and dried samples were packed into tin cups and analyzed with a PRISM II continuous flow isotope ratio mass spectrometer (CF-IRMS) to obtain $\delta^{34}S$ values (relative to V-CDT) (Giesemann et al., 1994). The precision in measuring $\delta^{34}S$ is $\pm$ 0.3 ‰ which is determined as the standard deviation (1σ) of $\delta^{34}S$ for several standard runs. $\delta^{34}S$ measurements were blank corrected using the sulfur concentration and $\delta^{34}S$ values for field blanks. Insufficient sulfate was present for some samples after concentration blank correction. Although the concentration of sulfate was too small to perform blank correction for some samples, they displayed the same range for $\delta^{34}S$ values as those which were blank corrected. This suggests little to no bias was introduced by blank correction. Therefore, $\delta^{34}S$ values are reported from some samples which were not isotopically blank corrected. These samples are indicated with a $*$ in Tables 1 and 2.

The PRISM II continuous flow isotope ratio mass spectrometer measures $\delta^{34}S$ and $\delta^{33}S$ simultaneously and the values for

non-enriched samples were expected to be related according to the Mass Dependent Fractionation (MDF) relation ($\delta^{33}S \sim 0.51\delta^{34}S$). For this experiment some of the samples were enriched in ^{34}S and they were identified by the use of the MDF relation between $\delta^{34}S$ and $\delta^{33}S$ of the standards for the same run. $\delta^{33}S/\delta^{34}S$ was averaged for standards for each run and $(\frac{\delta^{33}S}{\delta^{34}S}) - 2\sigma$ was used as a cutoff criteria and data falling below this criteria were tagged as enriched.

Care was taken to analyze sufficient standards and blanks between enriched samples (CIMS-ON periods) to ensure carryover was minimal. Little to no deviation in standards and blanks was apparent after enriched $\delta^{34}S$ values from CIMS-ON periods were analyzed. In this paper uncertainties are reported as 1σ standard deviation.

4.3 Natural tracer experiment

4.3.1 Sulfur ^{34}S release

The CIMS was operated between August 12, 12:00 to August 14, 12:00 and August 20th 12:00 to September 7th 9:45 local time. Ten standard cubic centimeter of 0.9 % $^{34}SO_2$ was diluted in 30 SLPM N_2 to obtain a mixing ratio of 3 ppm for $^{34}SO_2$ in the sample flow. $^{34}SO_2$ reacts with OH to form $H_2{}^{34}SO_4$ which is ionized by NO_3^- to form $H_2{}^{34}SO_4^-$ and $SO_4{}^{2-}$ ions that are detected at m/z=99 and m/z=49 in the negative ion spectrum of the mass spectrometer. An excess amount of $^{34}SO_2$ compared to the required $^{34}SO_2$ to complete titration of OH in the sample flow was used for ambient air OH reactivity measurements. Almost all of the flow entering was exhausted by the instrument which contained excess $^{34}SO_2$ and formed $H_2{}^{34}SO_4$. In one minute $n_{^{34}SO_2} = (7.4 \times 10^6) n_{H_2^{34}SO_4}$. Some of the formed $H_2{}^{34}SO_4$ is also lost by wall loss in the instrument so the majority of the exhaust is in the form of $^{34}SO_2$. For the periods when the CIMS was operational (CIMS-ON) significant ^{34}S isotope enrichment was observed; therefore, samples were divided into two sets, CIMS-ON and CIMS-OFF.

The first set is for samples collected during the shutdown periods of the CIMS (CIMS-OFF). These CIMS-OFF periods were used to investigate the isotopic composition of size segregated sulfate aerosols and SO_2 in the region and the possible sources and formation pathways of sulfate aerosols. The second set is for samples (CIMS-ON) affected by enriched ^{34}S and is not used as indicators of sulfur isotopic composition of sulfate aerosols in the region. Instead the enriched $^{34}SO_2$ is used as a natural tracer to follow the fate of SO_2 emitted from a local ground-based source and its oxidation.

4.3.2 Sulfur conversion ratio

In this paper we use the sulfur conversion ratio which is defined as the portion of SO_2 which is converted to particulate sulfate, and is defined as

$$F(s) = \frac{[SO_4]}{[SO_4] + [SO_2]}. \tag{6}$$

In this formula $[SO_4]$ is the concentration of sulfate aerosols with D<0.49 μm which is expected to be dominantly secondary sulfate aerosols according to Proemse et al. (2012a) and the absence of soil indicators.

Since F(s) is a measure of SO_2 to sulfate conversion it is a measure of oxidant loading. Therefore, significant positive correlation between F(s) and other compounds may be an indicator of the importance of that compound as a tracer for SO_2 oxidation.

This formula can be used for both CIMS-ON and CIMS-OFF periods since the number of enriched molecules reaching the high-volume sampler is very small and cannot change F(s). The number of enriched molecules reaching the high volume sampler is calculated using equations described in section 4.3.3 and the fraction of enriched molecules in comparison to the total sulfur concentration is reported in Table A1.

4.3.3 Concentration of ^{34}S enriched molecules

The concentration of enriched molecules as $^{34}SO_2$ and $^{34}SO_4$ were calculated using the following equations during CIMS-ON periods. Isotope ratio (R) values show the ratio of sulfur isotopes to the most abundant isotope which is ^{32}S for sulfur.

$$R^{34} = n^{34}S/n^{32}S \tag{7}$$

$$R^{33} = n^{33}S/n^{32}S \tag{8}$$

$$R^{36} = n^{36}S/n^{32}S \tag{9}$$

$$R^{34}_{enriched} = (n^{34}S + n^{34}S^*)/n^{32}S \tag{10}$$

$$n^{32}S + n^{33}S + n^{34}S + n^{36}S + n^{34}S^* = S_{total} \tag{11}$$

in which $n^{34}S^*$ is the number of ^{34}S atoms reaching the filter from the CIMS exhaust and S_{total} is the total number of sulfur atoms on the filter. R^{34} value is calculated as the average of R^{34} values for samples without enrichment. There were R^{33} data available from the IRMS but the uncertainty was high (± 3 ‰) and we used the value for the international standard for sulfur V-CDT. ^{36}S is included in calculations since the amount of $^{34}S^*$ from the CIMS exhaust is on the same order of magnitude. $R^{34}_{enriched}$ values were available for each sample. The concentration of sulfate for each sample was available from IC and the number of sulfur atoms as SO_2 or sulfate can be calculated. Then the number of ^{34}S from CIMS was calculated and divided by the volume of total sampled air and the number of $^{34}SO_2^*$ and $^{34}SO_4^*$ molecules per cm^3 was calculated (Table A1).

5 Results

5.1 Sulfur conversion ratio (F(s))

The sulfur conversion ratio (F(s) equation (6)) was calculated for the smallest size fraction of measured sulfate ($F_{<0.49\mu m}$). Absence of Ca and Mg on this size fraction (all concentrations were below the IC detection limit (0.1 mg/L)) indicated that primary soil particles were not present on this size fraction. Proemse et al. (2012a) suggested that less than 10% of total sulfur emissions from two major stacks in the region were primary sulfate in $PM_{2.5}$. Therefore, primary sulfate from stacks do not form a significant portion of sulfate aerosols in this size range since $F_{<0.49\mu m}$ fraction contains particles even in smaller sizes (D<0.49 μm) than 2.5 μm. Based on these two pieces of information it is expected that sulfate particles on this size fraction are mostly (>90%) secondary. As a result, F(s) gives valuable information about which pathways dominate SO_2 oxidation and formation of sulfate aerosols.

F(s) is not affected by enriched sulfate emissions during CIMS-ON periods (because the amount of $^{34}SO_2$ emitted was relatively small - Table A1). Hence, F(s) reflects conversion of SO_2 to sulfate for the entire measuring period. This implies negligible changes to F(s) values because of the CIMS emissions.

F(s) (CIMS-ON and CIMS-OFF) is plotted versus relative humidity in Figure 2. Positive correlations were observed for daytime and nighttime and daily samples (r = 0.88, r = 0.59, r = 0.58, respectively) with the same dependency (slope≃0.01). F(s)

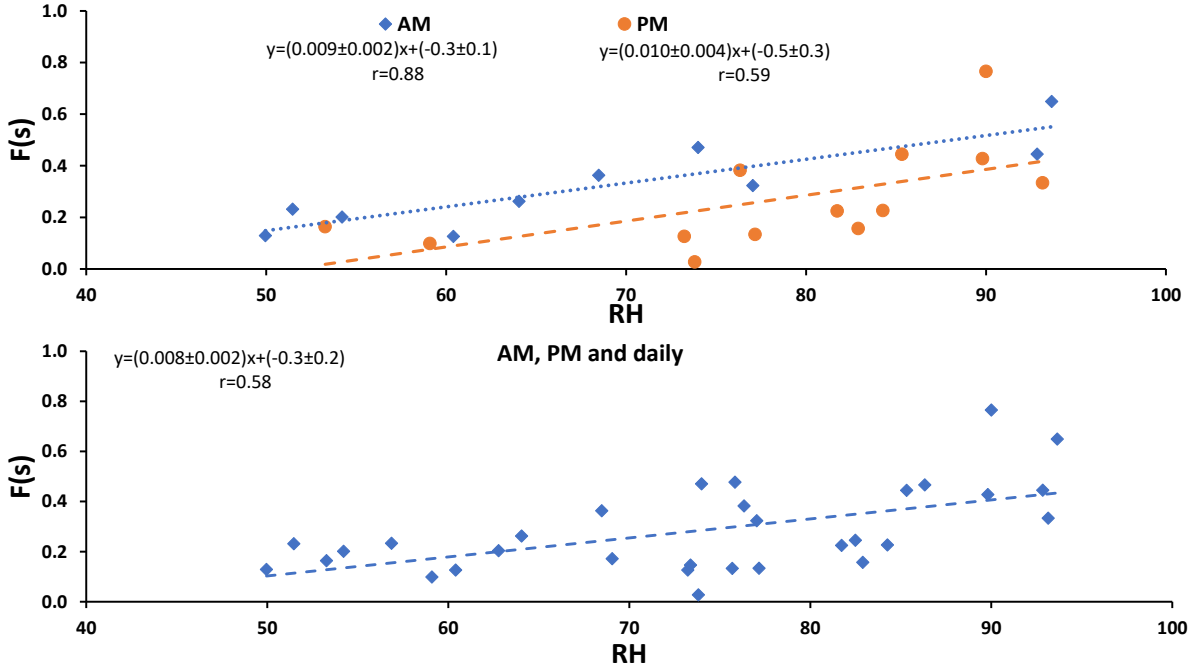

Figure 2. F(s) (CIMS-ON and CIMS-OFF) versus relative humidity. a) correlation during daytime and nighttime and b) correlation for daytime, nighttime and daily data. P-value<0.05.

values were usually higher during the daytime in comparison to nighttime values (Tables 1 and 2) which was what we expect for OH driven oxidation during daylight. In the troposphere, the OH radical is produced mainly from photolysis of O_3 to $O(^1D)$ and subsequent reaction with water vapor. If a steady state in $O(^1D)$ is assumed with respect to its production and loss, the (instantaneous) daytime OH production rate is proportional to $j(O^1D) \times [H_2O] \times [O_3]$. A negative correlation was observed between F(s) and this (integrated) OH production rate during the daytime (r = -0.72, P-value<0.05) (Figure A2). However, two data points with the highest RH (25 and 26 August) drive this correlation, and no correlation was observed for the remainder of the samples. This suggests that there may be SO_2 oxidation pathways in addition to OH during the day in this region.

The time series for SO_2 during the campaign is shown in Figure 3a. The time series was dominated by spikes in SO_2 mixing ratio. Phillips-Smith et al. (2017) used positive matrix factorization (PMF) to determine concentration time series for 5 factors during the campaign. This analysis showed that August 14, 23, 24 and September 3 and 4 were periods that the site was impacted by upgrader emissions. Concentrations of SO_2 , and Fe and Mn (measured in $PM_{2.5}$) were markedly higher during these periods (Figure 3).

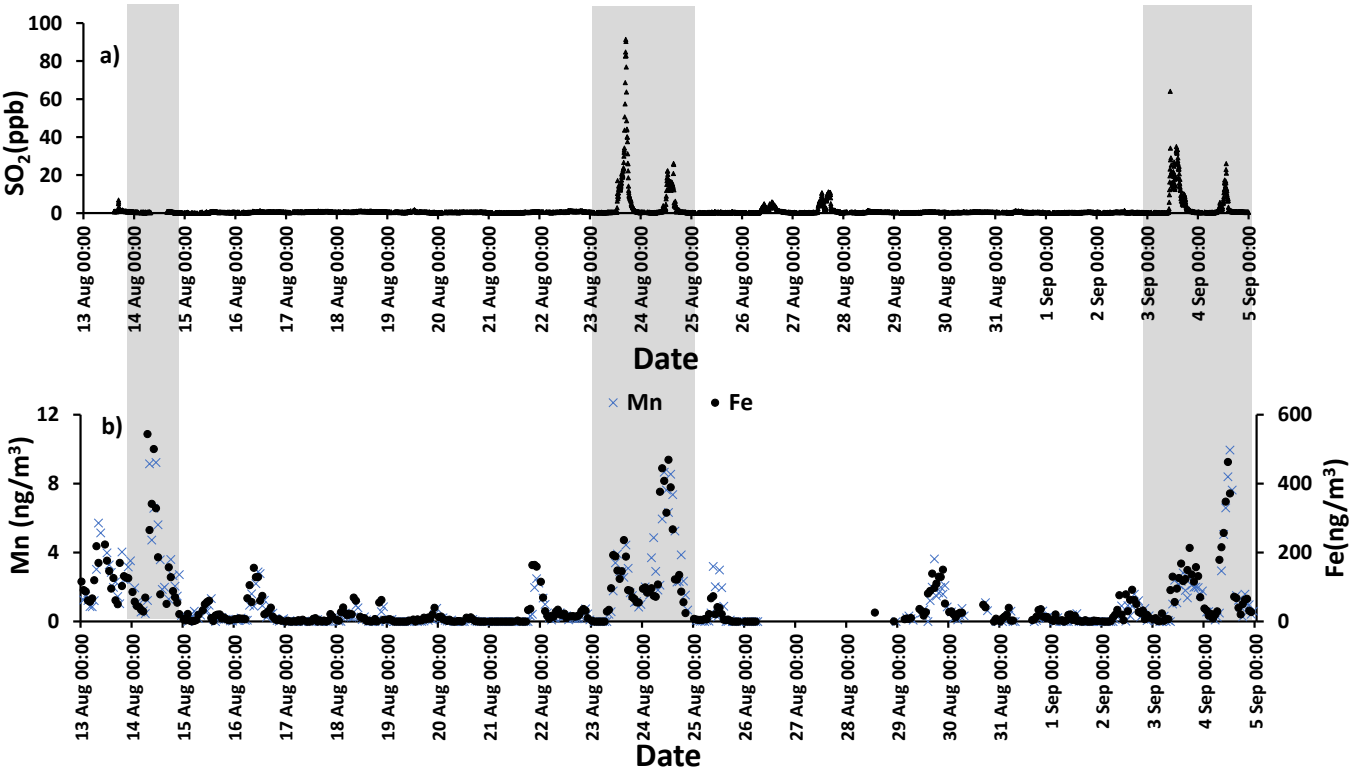

Figure 3. a) SO_2 time series with a sampling interval of five minutes (There is a gap in Aug 14 data) and b) hourly data for Mn (left axis) and Fe (right axis). Shaded areas indicate polluted periods.

It is interesting to note that F(s) for daytime was higher than nighttime for all samples except periods when the site was impacted by plumes from major oil sands upgrading facilities (polluted periods) (Phillips-Smith et al., 2017). A comparison

between AM and PM values for F(s) for August 23 and 24, showed that nighttime values were almost double the daytime values. F(s) value was not available for daytime of August 14 to compare with the nighttime value but August 14 PM showed the highest value for F(s) (0.77) during the entire campaign (Tables 1 and 2). At night, aqueous phase oxidation is the dominant SO_2 transformation pathway as OH is absent (Chin and Jacob, 1996). No correlation was observed between F(s) and O_3 mixing ratio for daytime, nighttime and daily samples (Figure A2). Therefore, it is expected that SO_2 oxidation occurs by H_2O_2 and/or the TMI-catalyzed pathway.

Fe and Mn concentrations, averaged over the night high-volume sampling periods, are shown in Figure A3. The averaged nighttime concentrations of Fe and Mn were higher during polluted periods (average values of 57 $\pm$ 20 (ng/m^3) and 1.5 $\pm$ 0.5 (ng/m^3), respectively) in comparison to other periods (average values of 9 $\pm$ 3 (ng/m^3) and 0.13 $\pm$ 0.06 (ng/m^3), respectively: Figure A3). The data collected on August 21 PM were excluded from this analysis because the PMF analysis by Phillips-Smith et al. (2017) showed this period to be distinct (discussed further below). To check if the TMI-catalyzed pathway played a role in SO_2 oxidation during nighttime, averaged concentrations of Fe and Mn were added and $[Fe+Mn] \times [H_2O]$ values were found and shown in Figure 4a. F(s) is also shown for nighttime samples (Figure 4b). It is observed that when $[Fe+Mn] \times [H_2O]$ value is high, F(s) is also high. Concentrations of Fe and Mn were associated with upgrader, soil, and haul road dust factors during polluted nighttime periods (Aug 14, 23, 24). Although August 21 PM is not a polluted period, it showed high $[Fe+Mn] \times [H_2O]$ values but F(s) is not high (Figure 4b). For August 21, the analysis by Phillips-Smith et al. (2017) showed that there was a peak for the soil factor but not upgrader and haul road dust. F(s) on this night was markedly lower than during periods when upgrader and haul road dust factors were high. F(s) for August 25 is also high since this is a rainy period (Section 4.1).

5.2 $\delta^{34}S$ values for size segregated sulfate aerosols and SO_2 during CIMS-OFF periods

During CIMS-OFF periods $^{34}SO_2$ emissions were absent, so $\delta^{34}S$ values reflect the sulfur isotopic composition of the sulfur compounds in the region and/or fractionation as the SO_2 is oxidized and transported to the AMS13 site. $\delta^{34}S$ values during CIMS-OFF periods for SO_2 and size segregated sulfate in size ranges $F_{<0.49\mu m}$, $E_{0.49-0.95\mu m}$, $D_{0.95-1.5\mu m}$, $C_{1.5-3.0\mu m}$, $B_{3.0-7.2\mu m}$ and $A_{>7.2\mu m}$ are shown in Table 1. Possible oxidation pathways of SO_2 to sulfate were investigated using these $\delta^{34}S$ values.

Blank corrected $\delta^{34}S$ values for SO_2 were +5.1 ‰ and +10.8 ‰. No negative $\delta^{34}S$ values were observed for SO_2. If it is assumed that no fractionation occurred during formation of primary sulfate in major stacks then it is expected that $\delta^{34}S$ values for SO_2 would be the same as primary sulfate (with an average of; +7.3 $\pm$ 0.3‰ and +9.4$\pm$ 2.0 ‰). The $\delta^{34}S$ values of SO_2 ranged from +5.1 ‰ to +11.1 ‰ (Table 1) and are consistent with this assumption. The lowest value (+5.1‰) is consistent with a $\delta^{34}S$ value for SO_2 from vehicle exhaust (Table 1).

$\delta^{34}S$ values for size $F_{<0.49\mu m}$ particles ranged between +1.8 ‰ and +15.1 ‰ with an average of +7.4 $\pm$ 4.2 ‰. Although this average overlaps with values given by Proemse et al. (2012b) for primary sulfate from the stack emissions (+7.3$\pm$ 0.3‰ and +9.4$\pm$ 2.0‰), there were $\delta^{34}S$ values lighter and heavier than what was expected from potential sulfur sources in the region

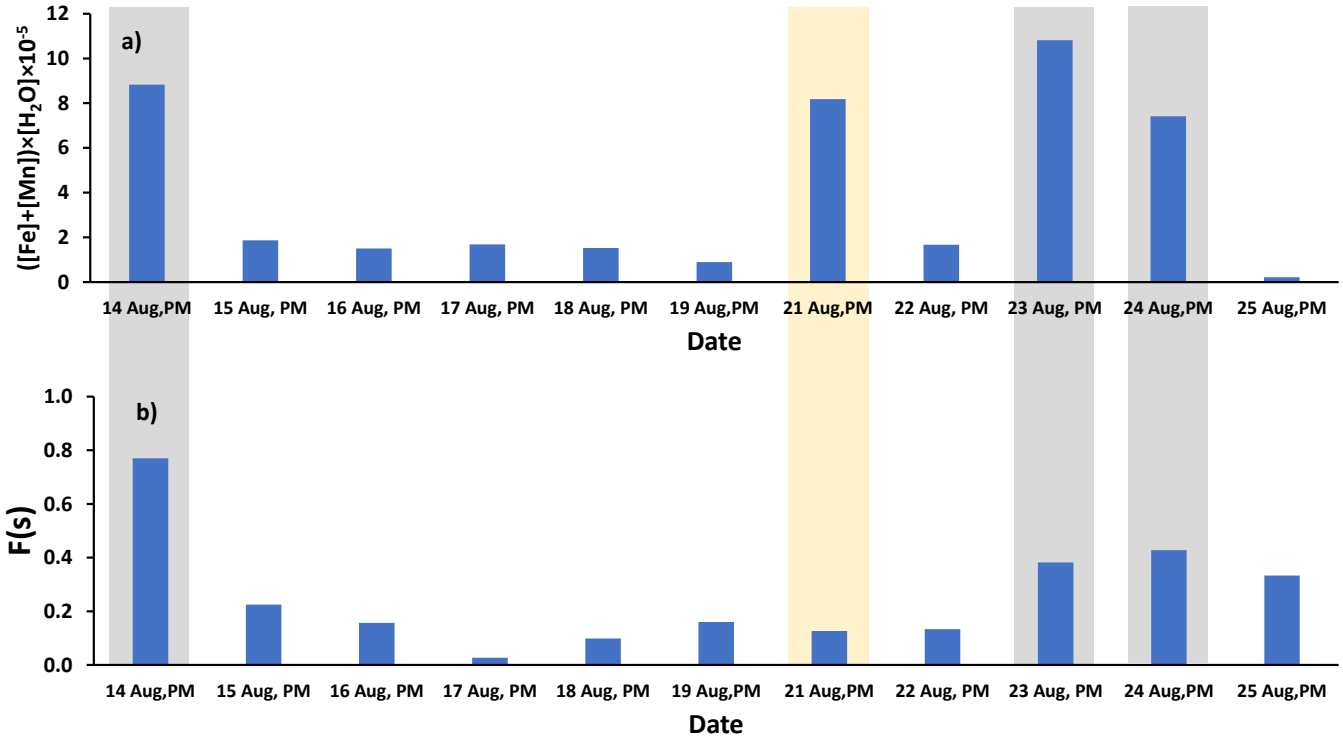

Figure 4. a) $([Fe]+[Mn])\times[H_2O]$ values for nighttime samples as an indicator of the TMI-catalyzed SO_2 oxidation pathway (Fe and Mn concentrations were averaged over the running periods of high-volume sampler) and b) F(s) values for the nighttime samples. Polluted periods and the soil episode are shown by grey and yellow shaded areas.

in this size range. Therefore, $\delta^{34}S$ of sulfate cannot be used as a quantitative indicator for industrial SO_2 emissions as isotope fractionation may have occurred as the stack emissions (SO_2) were transported to the AMS13 site. As shown in section 5.1 sulfate particles in this size range are predominantly secondary; therefore, these data can be used to investigate the importance of different SO_2 oxidation pathways during transport.

Particles in larger size ranges ($E_{0.49-0.95\mu m}$, $D_{0.95-1.5\mu m}$, $C_{1.5-3.0\mu m}$, $B_{3.0-7.2\mu m}$ and $A_{>7.2\mu m}$) are expected to contain more primary sulfate and had lower $\delta^{34}S$ values in comparison to the $F_{<0.49\mu m}$ size range. There were no negative values for sulfate particles in the size fraction $F_{<0.49\mu m}$, but negative values were observed for the size fraction $E_{0.49-0.95\mu m}$. All the available data for blank corrected size fractions $A_{>7.2\mu m}$ and $B_{3.0-7.2\mu m}$ were negative. There was a tendency to lighter $\delta^{34}S$ values for larger sulfate particles as shown in Figure 5.

Table 1. $\delta^{34}S$ (‰) values for SO_2, and sulfate aerosols in size ranges $F_{<0.49\mu m}$, $E_{0.49-0.95\mu m}$, $D_{0.95-1.5\mu m}$, $C_{1.5-3.0\mu m}$, $B_{3.0-7.2\mu m}$ and $A_{>7.2\mu m}$ during CIMS-OFF periods. Not blank corrected samples have the uncertainty of $\pm$ 0.3 ‰, and the uncertainty for blank corrected samples are shown in brackets.

Date	SO_2	F	E	D	C	B	A	F(s)	error in F(s)
14Aug,pm	+10.8	+4.6 (0.4)	+2.8 (3.5)	-	-	+2.1*	-	0.77	0.09
15Aug,am	+11.1*	+6.5 (0.8)	+6.5 (3.8)	+0.4*	-0.38*	-0.24*	-	0.47	0.06
15Aug,pm	-	+12.9 (2.0)	+2.2*	+1.5*	-	-0.33*	-4.1 (2.1)	0.22	0.04
16Aug,am	+5.1	+1.8 (0.8)	+6.5 (2.2)	+3.2*	-2.9*	-1.1*	-4.5 (1.4)	0.13	0.03
16Aug,pm	+7.4*	+8.9 (1.9)	-0.2*	-	-0.4*	+3.5*	-2.1 (1.1)	0.16	0.02
17Aug,am	-	+15.1 (2.1)	+6.3*	-1.1*	+1.5*	+1.8*	+0.74*	0.13	0.01
17Aug,pm	-	+9.0*	+1.3*	+0.1*	+3.3*	+2.1*	-1.2*	0.03	0.01
18Aug,am	+10.2*	+6.5 (1.7)	-1.7 (1.9)	-0.89*	-0.88*	-5.3 (2.2)	-0.56*	0.13	0.01
18Aug,pm	-	+6.1 (2.7)	+2.3 (5.0)	+2.1*	-1.0*	-1.8 (2.4)	-2.9*	0.10	0.01
19Aug,pm	-	+8.2 (1.1)	-0.6*	+2.6*	+5.4*	+1.6*	-0.67*	0.16	0.05

* not blank corrected samples

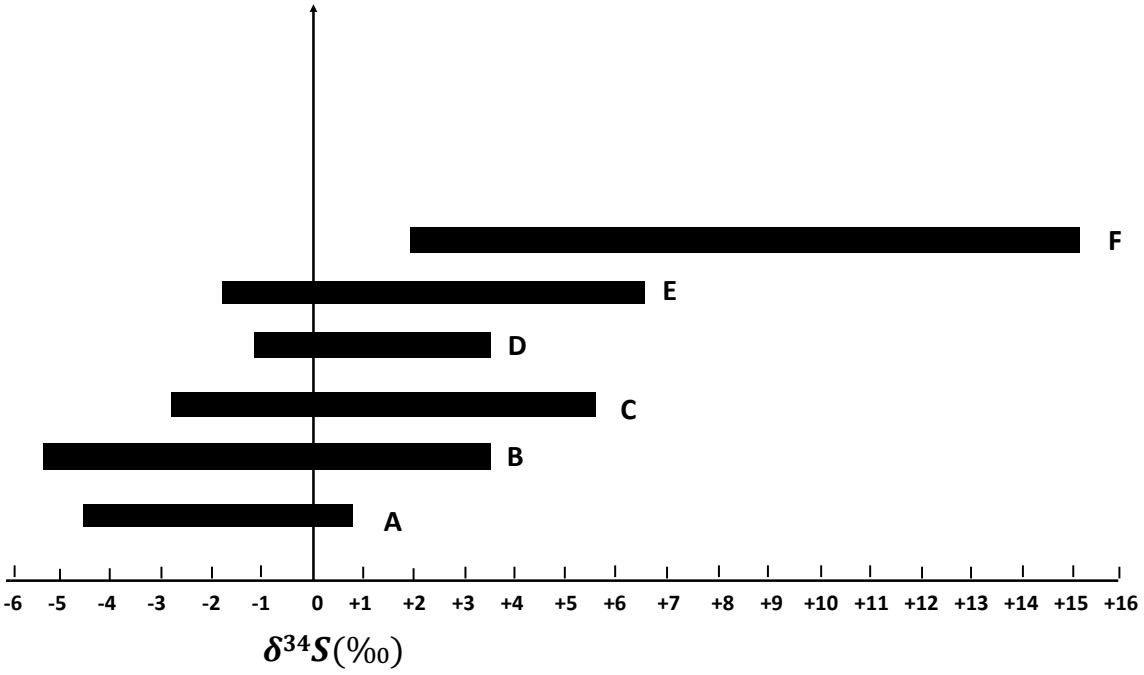

Figure 5. $\delta^{34}S$ ranges for $F_{<0.49\mu m}$, $E_{0.49-0.95\mu m}$, $D_{0.95-1.5\mu m}$, $C_{1.5-3.0\mu m}$, $B_{3.0-7.2\mu m}$ and $A_{>7.2\mu m}$ size ranges during CIMS-OFF periods. As the particles become larger, $\delta^{34}S$ becomes more negative.

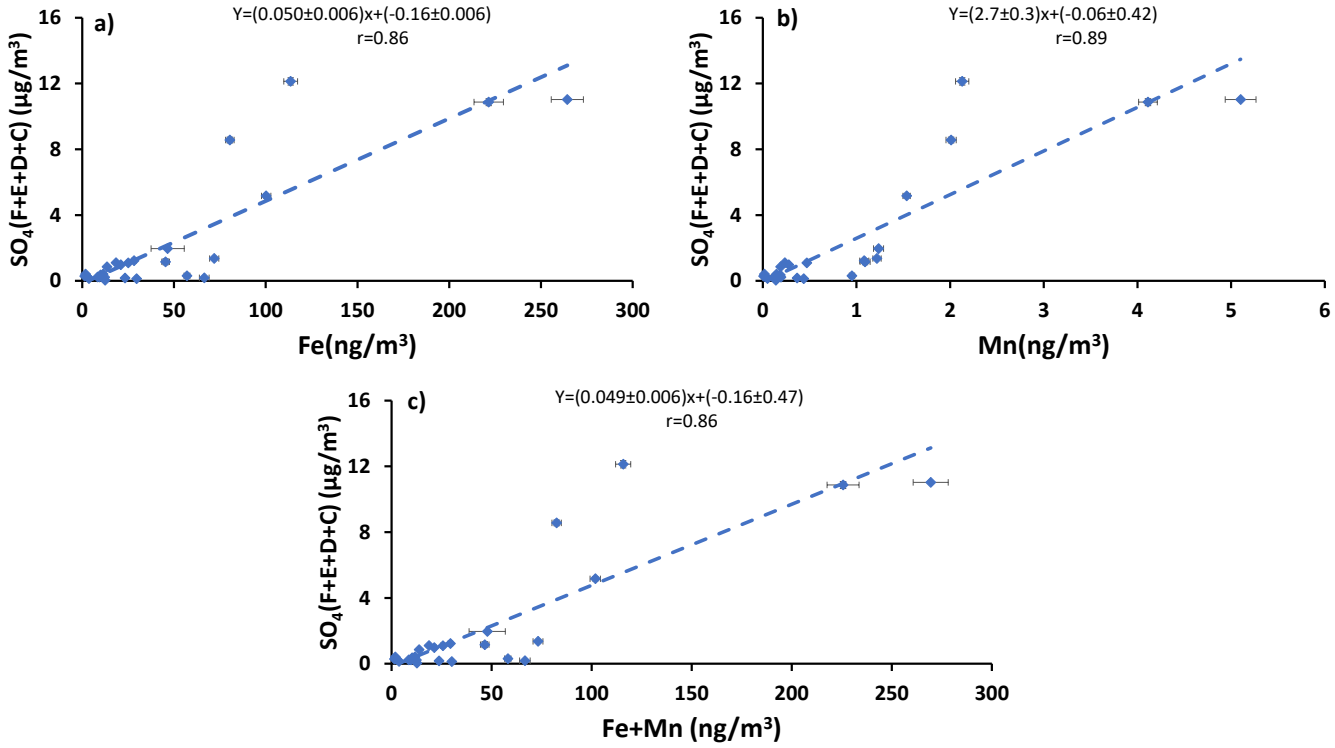

Figure 6. Sum of concentrations of sulfate in size ranges $F_{<0.49\mu m}$, $E_{0.49-0.95\mu m}$, $D_{0.95-1.5\mu m}$ and $C_{1.5-3.0\mu m}$ versus the concentration of a) Fe, b) Mn and c) Fe+Mn.

5.2.1 Correlation between Fe and Mn and sulfate concentration and $\delta^{34}S$ values during CIMS-OFF periods

Sulfur dioxide (SO_2) can be oxidized in the aqueous phase by O_2 in the presence of TMIs predominantly by Fe^{3+} and Mn^{2+}. If this is an important oxidation pathway more secondary sulfate may be produced when the concentrations of catalysts are higher. Concentrations of Fe and Mn were measured in $PM_{2.5}$ particles, therefore, the concentration of sulfate in size fractions $F_{<0.49\mu m}$, $E_{0.49-0.95\mu m}$, $D_{0.95-1.5\mu m}$, and $C_{1.5-3.0\mu m}$ were added to find the concentration of sulfate in particles with D<3 μm. The sulfate concentration in size range D<3 μm is almost the same as the concentration in $PM_{2.5}$ since the concentration in size fraction $C_{1.5-3.0\mu m}$ is very low (zero for all periods except polluted periods which ranges between 0.58 to 1.76 $\mu g/m^3$). The concentration for particles with D<3 μm is plotted versus Fe and Mn concentrations and the sum of Fe and Mn in Figure 6. Positive correlations were observed for all three cases (r = 0.86, r = 0.89, r = 0.86, respectively: Figure 6). Positive correlations were also observed when the concentrations of sulfate in the aerosol size fractions $F_{<0.49\mu m}$ and $E_{0.49-0.95\mu m}$ were plotted against the concentrations of Fe and Mn and the sum of Fe and Mn (Figure A4). There were not enough sulfate concentration data for size fractions $C_{1.5-3.0\mu m}$ and $D_{0.95-1.5\mu m}$ to show the individual correlations with Fe, Mn and the sum of Fe and Mn.

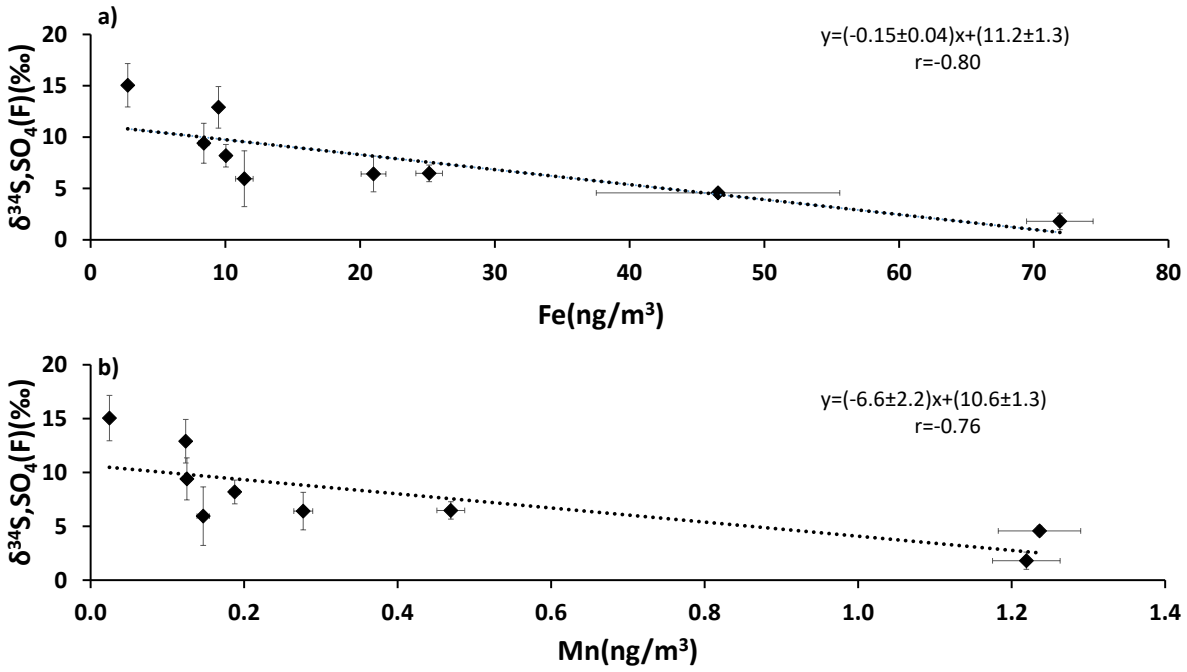

Figure 7. $\delta^{34}S$ values of size $F_{D<0.49\mu m}$ sulfate aerosols versus the concentrations of a) Fe and b) Mn

When SO_2 is oxidized by the TMI-catalyzed pathway the sulfur isotopic composition of the sulfate formed is lighter than the isotopic composition of the reactant SO_2. Significant anti-correlations were apparent for sulfate $\delta^{34}S$ values in size fraction $F_{<0.49\mu m}$ when plotted against Fe and Mn concentrations (r = -0.80 and r = -0.76, respectively: Figure 7). This suggests that lighter $\delta^{34}S$ values occur in secondary sulfate in the presence of higher concentrations of Fe and Mn. Insufficient isotope data were available to create similar plots for other size fractions. Positive correlations were also observed between concentrations of Fe and Mn and the concentration of SO_2 (r = 0.67 and r = 0.65, respectively: Figure A5) which may indicate that they originate from the same source, or were transported together to the sampling site.

5.3 $\delta^{34}S$ values of SO_2 and size segregated sulfate aerosols during CIMS-ON periods

The release of $^{34}SO_2$ from the CIMS allowed an examination of SO_2 oxidation to sulfate under field conditions. A very unexpected result was found: $\delta^{34}S$ values for SO_2 and sulfate samples with D<0.49 μm during the periods when the CIMS was operated (CIMS-ON) are shown in Table 2. The blank corrected data show that $\delta^{34}S$ values for enriched SO_2 samples were only as high as +35.6 ‰, and there were values without enrichment ranging between +4.8 ‰ and +10.9 ‰ with an average value of +8.3±1.8 ‰. All sulfate samples in size range $F_{<0.49\mu m}$ representing SO_2 oxidation during the CIMS-ON periods were blank corrected, and all AM and PM samples were highly enriched in ^{34}S; $\delta^{34}S$ values were as high as +913‰ (Table 2). A comparison between the isotopic composition of sulfate aerosols in size range $F_{<0.49\mu m}$ and SO_2 samples (R_{SO_4}/R_{SO_2})

Table 2. $\delta^{34}S$ values (‰) for SO_2 and sulfate with diameter $< 0.49\mu$m, and ratio of sulfate to SO_2 isotope during CIMS-ON periods, F(s) values and the error in F(s). Enriched samples were selected by comparing the mass dependent fractionation relation between $\delta^{34}S$ and $\delta^{33}S$ for the sample and standards at the same run. Average uncertainty for $\delta^{34}S$ values is $\pm$0.5 ‰.

Date	$\delta^{34}S_{SO_2}$	$\delta^{34}S_{SO_4}$	$\frac{R_{SO_4}}{R_{SO_2}}$	F(s)	error in F(s)
13Aug,am	+18.6^{*,a}	+155.8	-	-	-
14Aug,am	-	+47.1	-	-	-
20Aug,daily	+7.2*	+181.9	-	0.23	0.04
21Aug,pm	-	+441.6	-	0.13	0.02
22Aug,am	-	+409.5	-	0.23	0.02
22Aug,pm	+12.2^{a}	+572.6	1.553	0.13	0.02
23Aug,am	+4.8	+27.8	1.022	0.20	0.01
23Aug,pm	+18.4^{a}	+15.5	0.997	0.38	0.01
24Aug,am	+10.9	+26.8	1.015	0.26	0.01
24Aug,pm	+19.6^{a}	+88.7	1.068	0.43	0.06
25Aug,am	+8.6	+33.1	1.024	0.65	0.07
25Aug,pm	+8.4	+74.4	1.066	0.33	0.08
26Aug,am	+7.7	+21.5	1.014	0.45	0.01
26Aug,pm	+21.2^{a}	+48.2	1.026	0.44	0.02
27Aug,daily	+8.4	+21.5	1.012	0.47	0.01
28Aug,am	+13.0*	-	-	0.36	0.03
28Aug,pm	+10.2*	+298.1	-	0.23	0.04
29Aug,daily	+10.0	+56.9	1.046	0.25	0.04
30Aug,daily	+7.8*	+364.9	-	0.13	0.02
31Aug,daily	+35.6^{a}	+312.2	1.267	0.48	0.05
1Sep,daily	-	+913.3	-	0.17	0.04
2Sep,daily	+6.9*	+735.9	-	0.15	0.03
3Sep,daily	+7.8	+24.6	1.016	0.20	0.01
4Sep,daily	+26.94^{a}	-	-	-	-

a tagged as enriched

* not blank corrected samples. These are only shown for comparison, no calculation has been done using these values.

showed that the sulfate particles with D<0.49 μm were much more enriched in ^{34}S from the $^{34}SO_2$ tracer released by the CIMS. The concentration of enriched sulfur as $^{34}SO_2$ and $^{34}SO_4$ molecules per cm^3 is also calculated as described in section 4.3.3 and the data are reported in Table A1. Sulfate aerosols during CIMS-ON periods in the size ranges $E_{0.49-0.95\mu m}$, $D_{0.95-1.5\mu m}$, $C_{1.5-3.0\mu m}$, $B_{3.0-7.2\mu m}$ and $A_{>7.2\mu m}$ also showed enrichment for most of the samples (85 out of 100 samples showed enrich-

Table 3. $\delta^{34}S$ (‰) values for sulfate in size ranges $E_{0.49-0.95\mu m}$, $D_{0.95-1.5\mu m}$, $C_{1.5-3.0\mu m}$, $B_{3.0-7.2\mu m}$, and $A_{>7.2\mu m}$ during CIMS-ON periods. Average uncertainty for $\delta^{34}S$ values is $\pm$0.5 ‰.

Date	$\delta^{34}S_{SO_4}(E)$	$\delta^{34}S_{SO_4}(D)$	$\delta^{34}S_{SO_4}(C)$	$\delta^{34}S_{SO_4}(B)$	$\delta^{34}S_{SO_4}(A)$
13Aug,am	+25.7*	+31.5*	+45.2*	+54.1	+23.1
14Aug,am	+28.5*	+59.1	+75.1	+65.5	+49.0
20Aug,daily	+66.2	+28.5*	+35.2*	+30.3*	+30.8*
21Aug,pm	+31.0	+34.5*	+32.8*	+33.3*	+31.5
22Aug,am	+76.2	-	+111.4*	+110.3*	+46.1*
22Aug,pm	+55.8*	-	+61.4*	+67.5	+83.9*
23Aug,am	+37.4	+29.9	+31.1	+23.7	+28.7
23Aug,pm	+15.9	+12.5	+11.8*	+9.3*	+6.8
24Aug,am	+8.0	-	+29.2	+18.5	+10.2
24Aug,pm	+55.6	+15.9*	+21.6*	+22.1*	+39.5
25Aug,am	+12.0*	+15.5*	+12.2*	+16.9	+22.9*
25Aug,pm	+27.7*	+21.3*	+18.5*	+16.9*	+32.0*
26Augam	+15.8	+19.7	+41.4	+31.9	+28.9
26Aug,pm	+11.5[b]	-	+19.7*	+15.3*	+26.1*
27Aug,daily	+25.6	+19.9	+20.9*	+31.8	+32.6
28Aug,am	-	+217.1*	+201.3*	+212.1*	-
28Aug,pm	+224.8*	+310*	+211.2*	+240*	-
29Aug,daily	+80.3*	+98.5*	+85.1*	+71.9*	-
30Aug,daily	+188.9*	-	+194.9*	+176.5*	+217*
31Aug,daily	+166.8*	-	+537.7*	+341.8*	+339.5*
1Sep,daily	+372.2*	+132.9*	+825.1*	-	-
2Sep,daily	-	-	+483.4*	-	+274*
3Sep,daily	+45.8	+33.5*	+38.9*	+30.8*	+14.6*

* not blank corrected samples

ment) (Table 3).

Since the CIMS exhaust was located at the SE of the high-volume sampler, wind direction was considered as a potential factor in the analysis. No correlation (r = 0.16) was observed between the percent of time the high volume sampler was downwind of the CIMS exhaust and the concentrations of $^{34}SO_2$ or $^{34}SO_4$.

5.4 The role of Criegee biradicals in SO_2 oxidation

As mentioned in section 5.1 F(s) is higher during the daytime in comparison to nighttime except for polluted periods. No correlation (r = -0.36, excluding 25 and 26 August with the highest RH) was observed between F(s) and the integrated OH production rate, so there should be another possible oxidation pathway for SO_2 during daytime. One likely pathway is oxidation of SO_2 by Criegee biradicals.

Criegee biradicals are formed from ozonolysis of alkenes and may oxidize SO_2 to sulfate increasing F(s). Therefore, it is expected that correlations may exist between F(s) and precursors to Criegee biradicals. Significant positive correlations between F(s) and the concentration of α-pinene (r = 0.85), β-pinene (r = 0.87) and limonene (r = 0.82) were observed during daytime (Figure 8). No correlation was observed between F(s) and monoterpenes during nighttime.

The concentration of monoterpenes showed a negative correlation with the mixing ratio of O_3. There was a power law rela-

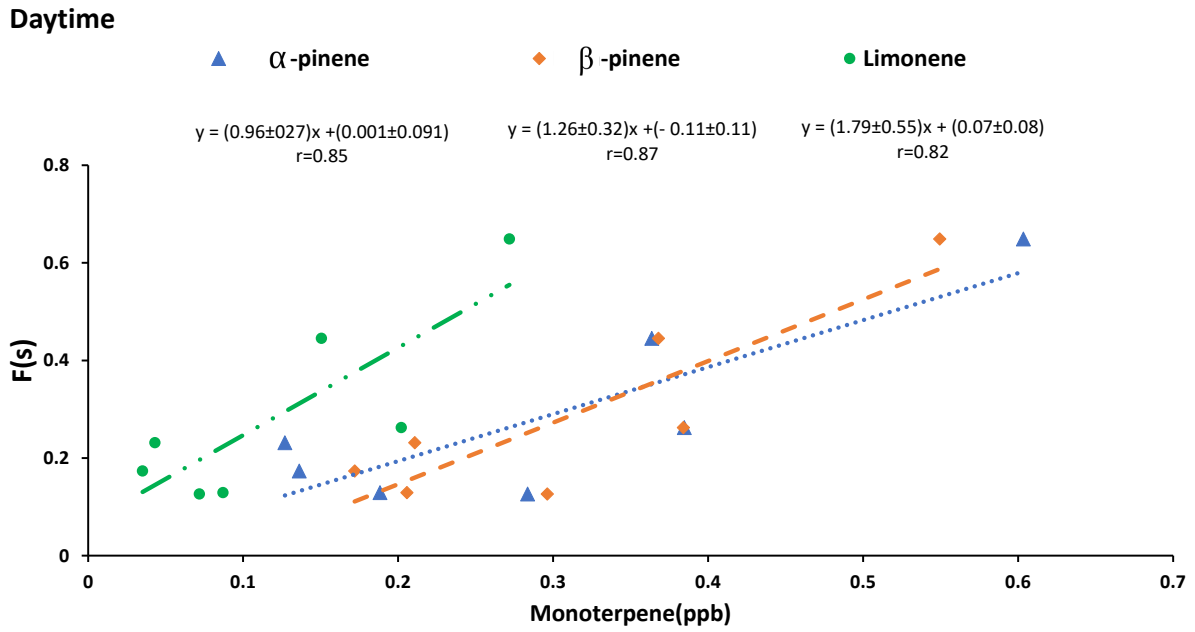

Figure 8. F(s) versus the concentration of α-pinene, β-pinene and limonene during daytime

tionship between monoterpenes and O_3 mixing ratio during the daytime and a linear dependency at night (r = -0.60) (Figure 9). Concentrations of other VOCs were only available as 24 hour averages. Most of the alkenes measured were found to be below the detection limit. Alkenes with concentrations higher than the detection limit except isoprene showed significant positive correlations with secondary sulfate aerosols (D<0.49 μm) and all of them except isoprene and tetrachloroethene showed significant correlations with SO_2 (Table A2).

Correlations with aromatic compounds generally fall into two categories. The first set includes compounds which are highly

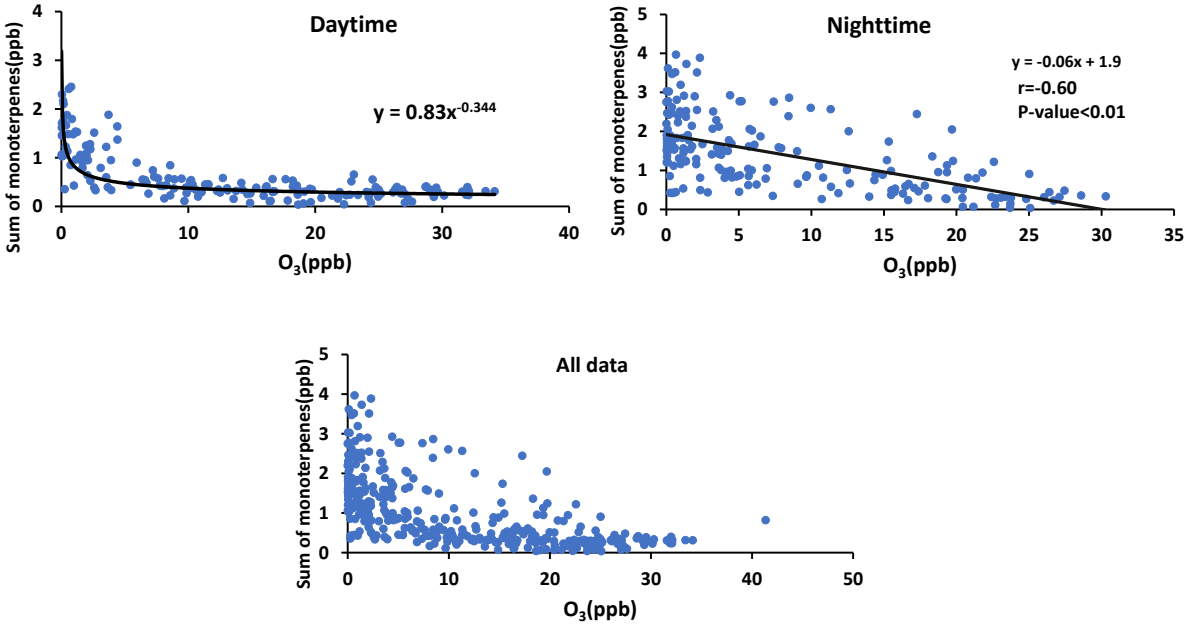

Figure 9. Sum of α-pinene, β-pinene and Limonene versus ozone mixing ratio for daytime and night time and all data.

correlated with SO_2 and sulfate with D<0.49 μm such as benzene. The second set contains the ones which show no such correlations but are correlated with F(s) (Table A3). Styrene and p-cymene are two compounds with no correlation with SO_2 and sulfate but significant correlations with F(s) (r = 0.58 for both, and r = 0.66 and r = 0.71, respectively when the rainy day data is omitted, P-value<0.05) (Table A3, Figure A6). They also show a positive correlation together (r = 0.71, P-value<0.05) (Figure A6).

6 Discussion

6.1 Potential TMI-catalyzed SO_2 oxidation

Sulfur conversion ratios (F(s)) and sulfur isotope data for SO_2 and size segregated sulfate aerosols were used to investigate the role of TMI-catalyzed SO_2 oxidation in the region.

F(s) is calculated for sulfate particles with D<0.49μm and showed significant positive correlations with RH for daytime, nighttime and daily data (Figure 2). A positive relationship between F(s) and RH is expected for both gas and aqueous phase SO_2 oxidation. Aqueous phase is the dominant oxidation pathway at night. The similar slopes for nighttime and daytime F(s) versus RH plots suggests that SO_2 aqueous phase oxidation may be an important oxidation pathway for both day and night and the offset (intercept that is higher for daytime than nighttime) suggests there is additional gas phase SO_2 oxidation that takes

place during the day.

Known aqueous phase oxidants for SO_2 are H_2O_2, O_3, and O_2 in the presence of TMIs. No correlation was observed between F(s) and O_3 mixing ratio, which indicates the minor importance of O_3 as an oxidant in aqueous phase. The pH dependency of aqueous O_3 oxidation of SO_2 makes this reaction very slow at low pH (pH<5.5). This reaction is also self-limiting and production of sulfate lowers the pH and slows down further reaction (Seinfeld and Pandis, 1998). Therefore, aqueous phase oxidation of SO_2 occurs mostly by H_2O_2 and/or O_2 in presence of TMIs.

The conversion ratio of SO_2 to sulfate (F(s)) was consistently higher during the day than at night except during polluted periods (Aug 14, 23 and 24). This is consistent with gas phase contributions to SO_2 oxidation in addition to aqueous phase oxidation that occurred both during the day and at night (Section 5.1). On polluted nights, the SO_2 to sulfate conversion ratio was twice as high as during the day and on Aug 14 at night the highest (0.77) conversion ratio for the entire campaign was observed (Tables 1 and 2). Averaged Fe and Mn concentrations on these polluted nights coincided with the highest values for SO_2 to sulfate conversion (F(s)) (Figure A3). In this campaign whenever both RH and the sum of Fe and Mn concentrations were high at night the proportion of SO_2 that was converted to sulfate (F(s)) was higher (Figure 4). These conditions of coincident high RH and Fe+Mn concentrations was met on polluted nights during the campaign. On these nights the ratio of Fe/Mn was consistent at around 40 (38, 40, 42 for Aug 14, 23, 24, respectively). This specific ratio may be a useful indicator for the source of Fe and Mn in aerosols. A particular night that was not classified as polluted (Aug 21) was identified as having Fe and Mn from soil (Phillips-Smith et al., 2017). The ratio of Fe/Mn on that night was 76, and the SO_2 to sulfate conversion ratio was indistinguishable from the remainder of the non-polluted nighttime samples (Figure 4). Therefore, it is reasonable to suggest that Fe/Mn around 40 is associated with a non-soil source. The two remaining sources are upgrader emissions and haul road dust. This interpretation of Fe and Mn on polluted nights as originating from anthropogenic emissions (Fe/Mn $\sim$ 40) rather than soil, is consistent with the higher solubility of anthropogenic TMIs relative to soil (Kumar et al., 2010).

Sulfur isotope measurements can provide the means to distinguish TMI from H_2O_2 aqueous oxidation. Isotope fractionation will be evident in sulfate when a large reservoir of SO_2 (e.g. from stack emissions) mixes with oxidants during transport and produces accumulated sulfate product captured over 12 or 24 hours. So long as the fraction of reaction is low (<30$\%$) the difference in $\delta^{34}S$ values for SO_2 and sulfate will reflect the magnitude and direction of the fractionation process. For the TMI-catalyzed pathway this direction is negative and produces lighter sulfate than SO_2. This directly contrasts with fractionation for O_3, H_2O_2, and OH oxidation pathways. Evidence that SO_2 released from tall stacks is transported high above the ground and mixes down toward the surface at AMS13 has been demonstrated by Gordon et al. (2017) and should provide conditions meeting the requirement for fraction of reaction <30$\%$ described here. The observed $\delta^{34}S$ values for size segregated sulfate aerosols in this study were consistent with aqueous TMI rather than H_2O_2 oxidation. Light $\delta^{34}S$ values for sulfate aerosols were observed in the region in comparison to other potential atmospheric sulfur sources. An alternate explanation for isotopically light $\delta^{34}S$ values in sulfate was proposed by Proemse et al. (2012b). Isotopically light $\delta^{34}S$ values (-3.9‰ and +0.3‰) were reported by this group for sulfate from bulk and throughfall deposition (deposition of excess water onto the ground surface from wet leaves) in the Athabasca oil sands region, consistent with the observations in this study. Since these values were lighter than the potential sources in the region, this showed evidence for a contribution of sulfate from a ^{34}S depleted source.

They suggested that the low $\delta^{34}S$ values observed for atmospheric sulfate collected at two sites were due to H_2S emitted from tailing ponds. Tailing ponds were in close proximity to the two sites where low $\delta^{34}S$ values were found. Proemse et al. (2012b) suggested that H_2S was oxidized to SO_2 and subsequently formed sulfate that then contributed to local sulfate deposition. The average value for $\delta^{34}S$ of SO_2 during CIMS-ON and CIMS-OFF (non enriched values) periods was +7.9 $\pm$ 2.1 ‰. This value is in the range of $\delta^{34}S$ of primary sulfate from two major stacks (Proemse et al., 2012a). No negative values were observed for $\delta^{34}S$ of SO_2. Also the opposite pattern to that observed in Figure 5, where larger size aerosols exhibit more negative $\delta^{34}S$ values than smaller size aerosols, is expected if H_2S were a significant source of sulfate at AMS13. The reason is that isotopically light SO_2 from H_2S oxidation is expected to produce secondary sulfate aerosols (from both homogeneous and heterogeneous reactions) in the smaller size fractions ($F_{<0.49\mu m}$ and $E_{0.49-0.95\mu m}$) with isotopically light $\delta^{34}S$ values. The larger $A_{>7.2\mu m}$ and $B_{3.0-7.2\mu m}$ size aerosols contain primary sulfate from soil and would reflect $\delta^{34}S$ values for untreated oil sand (+6.4 ‰; Proemse et al. (2012a)) in addition to sulfate from H_2S oxidation so they would have progressively more positive $\delta^{34}S$ values. Therefore, the contribution of significant amounts of H_2S to isotopically light samples through an SO_2 oxidation pathway is ruled out and there should be another reason for $\delta^{34}S$ values which were lighter than the expected sources in the region.

Primary sulfate and SO_2 can originate from haul road dust or Diesel exhaust. $\delta^{34}S$ values for these two sources are +5 ‰ and higher (Norman, 2004; Norman et al., 2004). Therefore, if haul road dust and Diesel primary sulfate were transported with Fe and Mn then $\delta^{34}S$ values should converge to +5 ‰ or higher. This should be particularly evident for the larger size aerosols ($A_{>7.2\mu m}$ and $B_{3.0-7.2\mu m}$). In fact the opposite is observed in Figure 5. Isotopically light $\delta^{34}S$ values for sulfate aerosols in size ranges $E_{0.49-0.95\mu m}$, $D_{0.95-1.5\mu m}$, $C_{1.5-3.0\mu m}$, $B_{3.0-7.2\mu m}$ and $A_{>7.2\mu m}$ were observed during CIMS-OFF periods. These values indicate that there was no, or only a very small contribution, of primary sulfate from major stacks. This leaves SO_2 from upgrader emissions as the most probable source of sulfate both for $F_{<0.49\mu m}$ size aerosols and for secondary sulfate formed on larger aerosol size fractions. $\delta^{34}S$ values reflect isotope fractionation during oxidation of SO_2 rather than source signatures. This is supported by a positive correlation between the sum of sulfate in size fractions $F_{<0.49\mu m}$, $E_{0.49-0.95\mu m}$, $D_{0.95-1.5\mu m}$, and $C_{1.5-3.0\mu m}$ and the concentrations of Fe and Mn and sum of Fe and Mn (r = 0.86, r = 0.89, and r = 0.86, respectively). The concentration of sulfate in size fractions $F_{<0.49\mu m}$, and $E_{0.49-0.95\mu m}$ also showed positive correlations with the concentration of Fe and Mn. This indicates that when Fe and Mn were prevalent present in aerosols either more sulfate can be formed or Fe and Mn were transported to AMS13 with SO_2 from a common emission source, likely upgrader emissions. There were also anti-correlations between $\delta^{34}S$ values of sulfate in size fraction $F_{<0.49\mu m}$ and the concentrations of Fe and Mn. This shows that lighter $\delta^{34}S$ values are associated with secondary sulfate formation and higher concentrations of Fe and Mn. One possible explanation for these observations may be the TMI-catalyzed SO_2 oxidation pathway during transport to the AMS13 site.

6.2 CIMS-ON

Little $^{34}SO_2$ reached the SO_2 filter in the high-volume sampler since high sulfur isotope enrichment was not observed for SO_2 samples (max $\delta^{34}S$ = 35.6 ‰). Instead $^{34}SO_2$ was oxidized to sulfate either as it moved in the atmosphere or on the filters in

the high-volume sampler. This result was completely unexpected since previous studies of $\delta^{34}S$ for sulfate and SO_2 showed no evidence of oxidation when SO_2 passed through the filters under marine or continental conditions (Ghahremaninezhad et al., 2016). The lack of $^{34}SO_2$ and the predominance of ^{34}S molecules on sulfate aerosols demonstrates an oxidation pathway that is rapid and specific to the conditions at the AMS13 site.

6.3 Potential oxidation of SO_2 by Criegee biradicals

The proportion of sulfate from SO_2 oxidation, F(s), during daytime, is generally larger than F(s) at night (Tables 1 and 2). Greater vertical mixing is expected during the day than at night. Stack emissions high above ground (Gordon et al., 2017) undergo oxidation during transport to the AMS13 site. Aloft, conventional oxidation pathways (i.e., OH driven oxidation) are likely more important than near the surface. At the same time precursors to Criegee biradicals will be released and mixed upward. A larger F(s) during the day than at night suggests that during daytime gas phase SO_2 oxidation occurs in addition to aqueous phase oxidation. Typically, OH is expected to dominate gas phase SO_2 oxidation during the day. However, the absence of a correlation between F(s) and integrated OH production rate ($j(O^1D)\times[H_2O]\times[O_3]$) indicates that the oxidation of SO_2 by OH was relatively minor in this campaign. However, a positive correlation between F(s) and α-pinene, β-pinene and limonene was observed during the day but not at night (Figure 8). This, combined with the loss of monoterpenes as daytime O_3 mixing ratio increased, suggests Criegee biradicals may be an important factor in SO_2 oxidation during daytime. Monoterpenes are oxidized by O_3 to form Criegee biradicals which can be stabilized and oxidize SO_2 to form secondary sulfate. This pathway is potentially more important during the day but less so at night. At night, the emissions of monoterpenes continue into a shallow nocturnal boundary layer that is decoupled from the residual layer above it. The terpenes then titrate O_3 at the surface, leading to the observed anti-correlation and low surface O_3 mixing ratio which limits Criegee biradical production.

Reaction between O_3 and anthropogenic alkenes may also generate Criegee biradicals, potentially leading to higher SO_2 to sulfate conversion ratio (F(s)). Many anthropogenic alkenes and aromatics likely have sources in common with SO_2 since a correlation (P-value<0.05) was observed between them (Tables A2 and A3). Their emissions are likely injected into (and transported within) layers above the measurement site and only sporadically entrain to the surface during daytime. When this happens, relationships between F(s) and anthropogenic alkenes may be observed. Styrene and p-cymene did not correlate with SO_2 or secondary sulfate but they were correlated with F(s) (r = 0.66, r = 0.71, respectively). Styrene reacts predominantly with OH but it can undergo ozonolysis to form Criegee biradicals. Styrene and p-cymene were also highly correlated with each other (r = 0.71) suggesting they were originating from the same source or sources. It is likely that styrene and p-cymene are indicators of other anthropogenic alkenes that facilitate SO_2 oxidation (for instance, tetrachloroethene).

7 Conclusions

Sulfur dioxide (SO_2) and size segregated sulfate aerosol concentrations and sulfur isotope compositions were measured during summer 2013 at the AMS13 site in the Athabasca oil sands region to investigate SO_2 oxidation pathways.

$\delta^{34}S$ values, F(s) and the relationship between secondary sulfate concentrations and Fe and Mn (in $PM_{2.5}$) show that there is

the potential that a significant proportion of SO_2 is oxidized during both the day and at night through aqueous phase oxidation by TMI catalysis. This is the first study to show that TMI-catalyzed oxidation of SO_2 as it is transported above and within the boundary layer is a potentially important pathway for sulfate formation in a strongly polluted environment during summer. The fraction of secondary sulfate was higher during the night than during the day for periods when the site was impacted by industrial plumes mixing downward from above. This, taken together with the high Fe and Mn concentrations at night shows the importance of aqueous phase reactions, probably by the TMI pathway as SO_2 is transported from the stack to the site at night. In addition, a natural tracer experiment with enriched ^{34}S demonstrated that oxidation of SO_2 on the surface of aerosols can be faster than expected. The results also show the potential importance of Criegee biradicals to daytime oxidation of SO_2 under highly polluted conditions.

Appendix A

Table A1. The fraction of enriched ^{34}S in sulfate samples in size $F_{<0.49\mu m}$ and the number of enriched sulfur molecules per cm^3 ($\frac{molecules(S)}{cm^3}$) for SO_2 and sulfate during CIMS-ON periods.

Date	$n^{34}S^*/totalS$	$\frac{n^{34}S^*(SO_2)}{V_{air}}$ ($\times 10^3$)	$\frac{n^{34}S^*(SO_4)}{V_{air}}$($\times 10^4$)
13Aug,am	0.006	-	1.8
14Aug,am	0.002	-	4.0
20Aug,daily	0.007	-	0.6
21Aug,pm	0.02	-	1.0
22Aug,am	0.02	-	2.6
22Aug,pm	0.02	0.3	1.7
23Aug,am	0.0008	0	2.1
23Aug,pm	0.0003	2.9	0.7
24Aug,am	0.0008	0	1.4
24Aug,pm	0.003	3.9	0.8
25Aug,am	0.001	0	0.4
25Aug,pm	0.003	0	0.3
26Aug,am	0.002	0	2.0
26Aug,pm	0.0006	0.7	0.3
27Aug,daily	0.0006	0	1.1
28Aug,am	-	-	-
28Aug,pm	0.01	-	1.1
29Aug,daily	0.002	2.0	-
30Aug,daily	0.015	-	0.8
31Aug,daily	0.013	0.4	3.3
1Sep,daily	0.037	-	1.7
2Sep,daily	0.029	-	1.2
3Sep,daily	0.0007	0	1.1
4Sep,daily	-	13	-

Table A2. Correlation coefficients (r) between SO_2, sulfate and alkenes with concentrations higher than the detection limit. P-values < 0.05 for all values except the ones shown with *.

	$SO_4{}^{2-}$	SO_2	F(s)
Ethene	0.59	0.52	0.45*
Propene	0.70	0.69	0.29*
Isobutene	0.77	0.68	0.33*
3-Methyl-1-Butene	0.78	0.71	0.40*
isoprene	0.02*	0.03*	0.002*
Tetrachloroethene	0.72	0.40*	0.53

* P-values > 0.05

Table A3. Correlation coefficients (r) between selected aromatics (At least 15 data points out of 20 data points are above the detection limit) and SO_2 and sulfate. P-values < 0.05 for all values except the ones shown with *.

Aromatics	SO_4^{2-}	SO_2	F(s)
Benzene	0.73	0.47	0.45*
Ethylbenzene	0.85	0.63	0.42*
m,p-Xylene	0.85	0.65	0.39*
o-Xylene	0.86	0.65	0.41*
Styrene	0.06*	0.07*	0.58
p-cymene	0.23*	0.02*	0.58

* P-values > 0.05

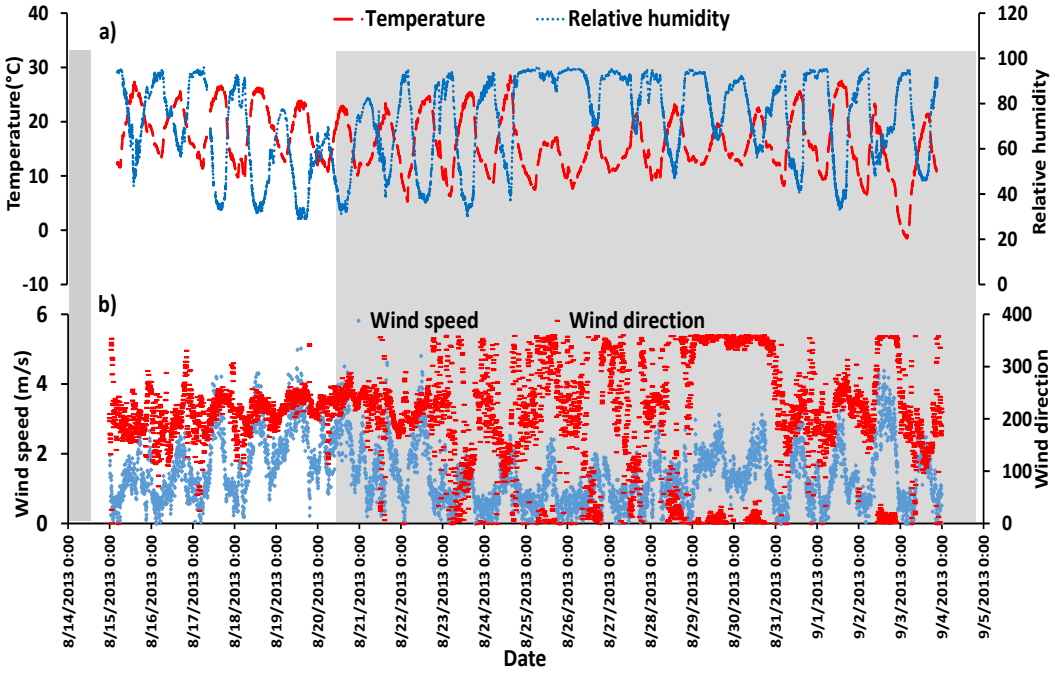

Figure A1. a) Temperature and relative humidity data with one minute sampling interval. b) Wind speed and wind direction with the sampling time interval of 5 minutes (data from WBEA meteorological station AMS13). Highlighted parts show the CIMS-ON periods.

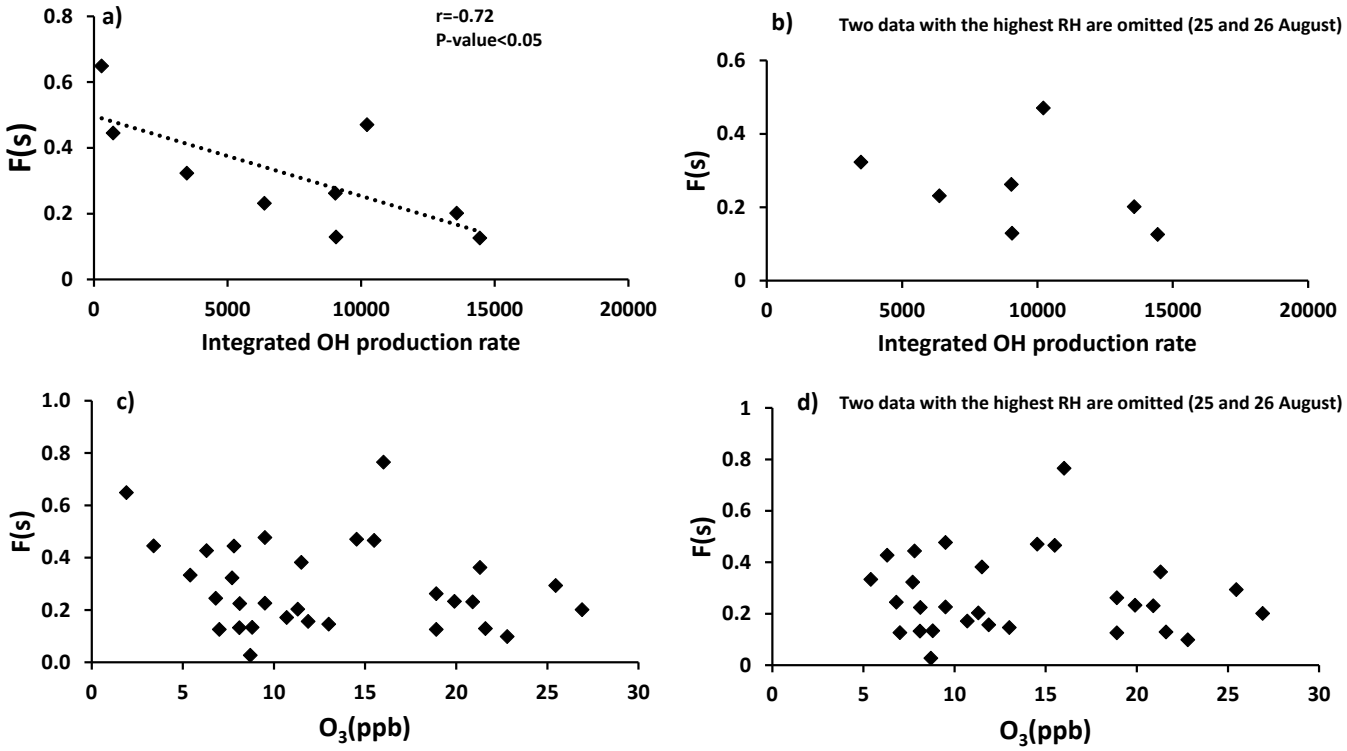

Figure A2. Sulfur conversion ratio F(s) versus a) integrated OH production rate for all available daytime data, b) integrated OH production rate when 25 and 26 August data with highest RH are omitted, c) O_3 with daytime, nighttime and daily data, and d) O_3 with all data when 25 and 26 August data with highest RH are omitted.

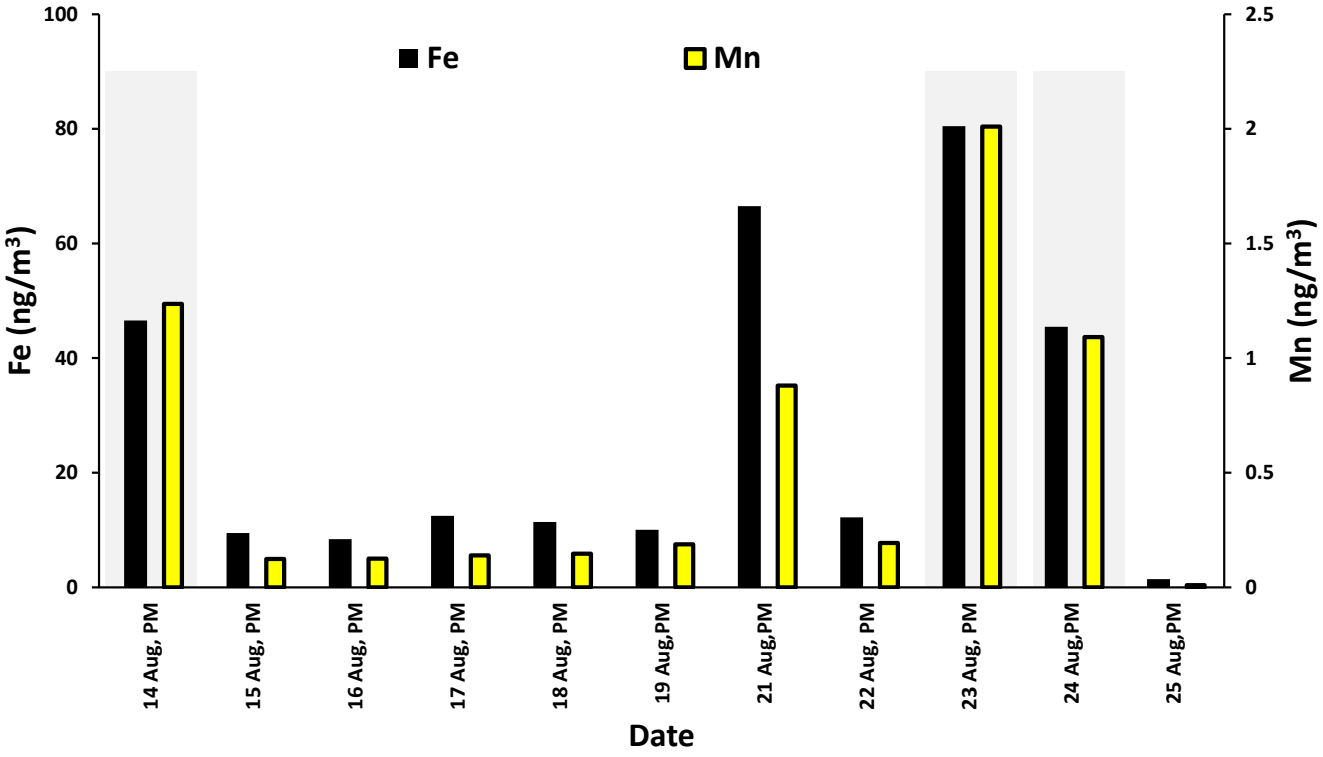

Figure A3. Concentrations of Fe and Mn during nighttime averaged on high-volume sampler running periods.

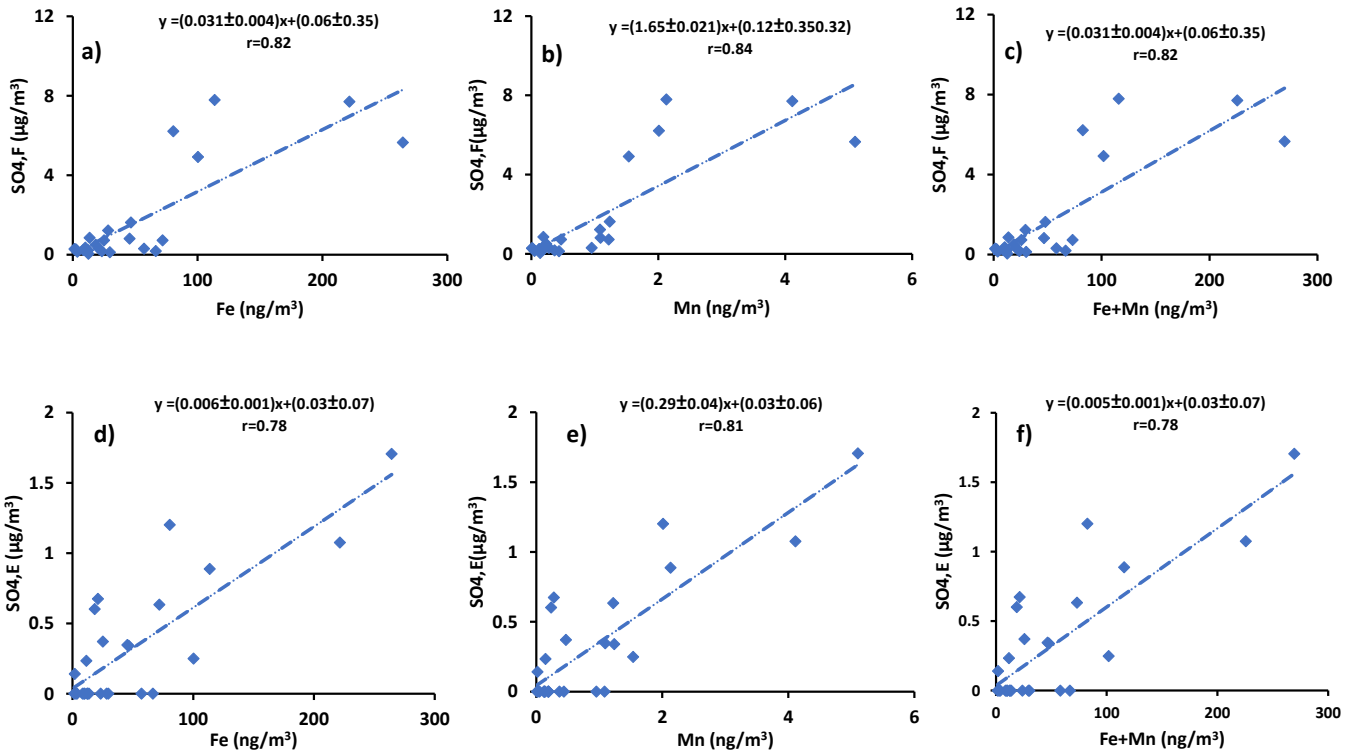

Figure A4. a), b) and c) SO_4 in size fraction $F_{<0.49\mu m}$ versus the concentrations of Fe and Mn measured in $PM_{2.5}$ and the addition of Fe and Mn. d), e) and f) SO_4 in size fraction $E_{0.49-0.95\mu m}$ versus the concentrations of Fe and Mn measured in $PM_{2.5}$ and the addition of Fe and Mn.

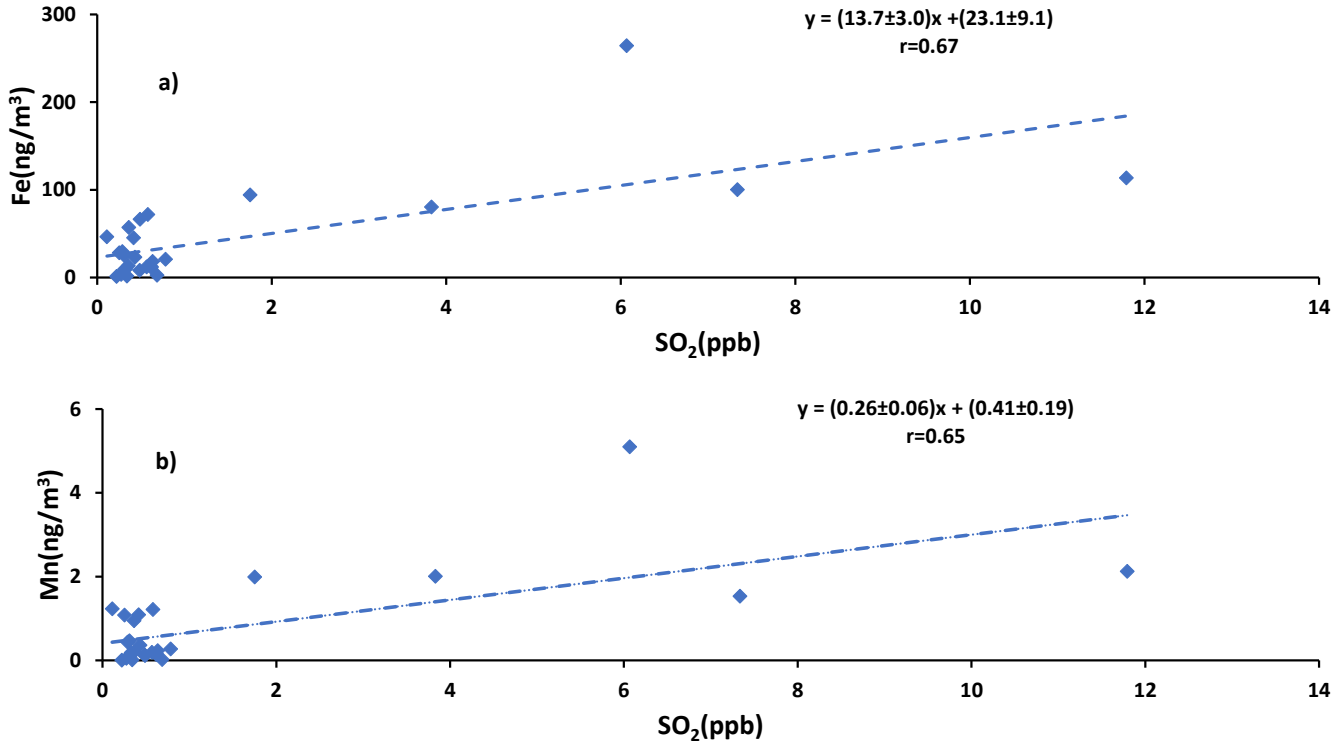

Figure A5. Concentrations of a) Fe and b) Mn measured in $PM_{2.5}$ versus the concentration of SO_2

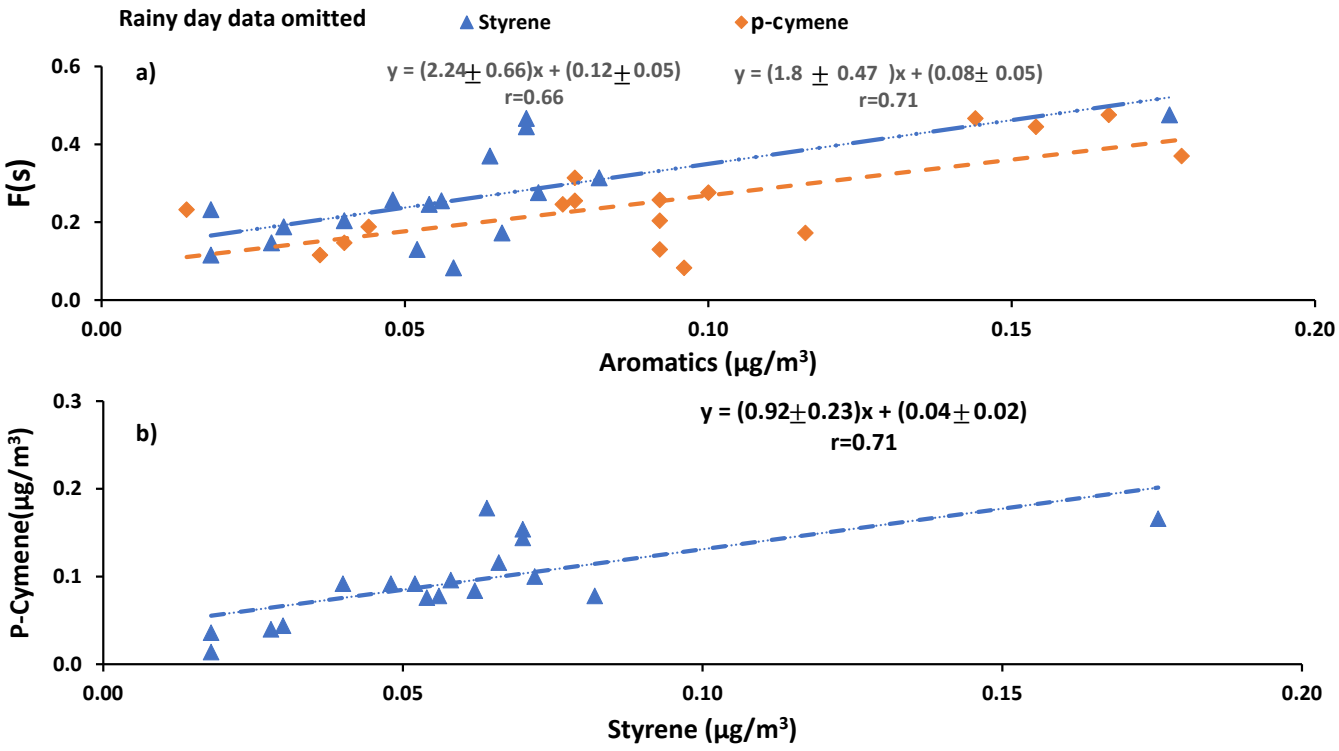

Figure A6. a) F(s) versus the concentration of styrene and p-cymene b) p-cymene versus styrene

Acknowledgements. This project was funded by Environment Canada under Joint Canada-Alberta Implementation Plan for Oil Sands Monitoring (JOSM) and NSERC. We would like to thank Jeff Brook and Daniel Wang from Environment Canda for VOC measurements and Greg Evans and Cheol-Heon Jeong from University of Toronto for their data on Fe and Mn concentrations. We also thank Jeremy Wentzell from Environment Canada for his assistance in defining working periods of CIMS.

References

Bardouki, H., Berresheim, H., Vrekoussis, M., Sciare, J., Kouvarakis, G., Oikonomou, K., Schneider, J., and Mihalopoulos, N.: Gaseous (DMS, MSA, SO_2, H_2SO_4 and DMSO) and particulate (sulfate and methanesulfonate) sulfur species over the northeastern coast of Crete, Atmos. Chem. Phys. Discuss., 3, 3869–3906, https://doi.org/10.5194/acpd-3-3869-2003, 2003.

Benson, D. R., Young, L.-h., Kameel, F. R., and Lee, S.-h.: Laboratory-measured nucleation rates of sulfuric acid and water binary homogeneous nucleation from the SO_2+OH reaction, Geophys. Res. Lett., 35, L11 801, https://doi.org/10.1029/2008GL033387, 2008.

Berglen, T. F.: A global model of the coupled sulfur/oxidant chemistry in the troposphere: The sulfur cycle, J. Geophys. Res., 109, D19 310, https://doi.org/10.1029/2003JD003948, 2004.

Berndt, T., Jokinen, T., Mauldin, R. L., Petäjä, T., Herrmann, H., Junninen, H., Paasonen, P., Worsnop, D. R., and Sipilä, M.: Gas-Phase Ozonolysis of Selected Olefins: The Yield of Stabilized Criegee Intermediate and the Reactivity toward SO_2, J. Phys. Chem. Lett., 3, 2892–2896, https://doi.org/10.1021/jz301158u, 2012.

Berresheim, H.: Gas-aerosol relationships of H_2SO_4 , MSA, and OH: Observations in the coastal marine boundary layer at Mace Head, Ireland, J. Geophys. Res., 107, 8100, https://doi.org/10.1029/2000JD000229, 2002.

Berresheim, H., Wine, P., and Davis, D.: Sulfur in the atmosphere, in Composition, Chemistry, and Climate of the Atmosphere, Van Nostrand Reinhold, New York, pp. 251–307, 1995.

Boucher, O. and Lohmann, U.: The sulfate-CCN-cloud albedo effect., Tellus B, 47, 281–300, https://doi.org/10.1034/j.1600-0889.47.issue3.1.x, 1995.

Boy, M., Mogensen, D., Smolander, S., Zhou, L., Nieminen, T., Paasonen, P., Plass-Dülmer, C., Sipilä, M., Petäjä, T., Mauldin, L., Berresheim, H., and Kulmala, M.: Oxidation of SO_2 by stabilized Criegee intermediate (sCI) radicals as a crucial source for atmospheric sulfuric acid concentrations, Atmos. Chem. Phys., 13, 3865–3879, https://doi.org/10.5194/acp-13-3865-2013, 2013.

Brimblecombe, P., Hammer, C., Rodhe, H., Ryaboshapko, A., and Boutron, C. F.: Human influence on the sulfur cycle. In Evolution of the Global Biogeochemical Sulphur Cycle, Wiley, Chichester, 39, 77–121, 1989.

Burkholder, J. B., Sander, S. P., Abbatt, J., Barker, J. R., Huie, R. E., Kolb, C. E., Kurylo, M. J., Orkin, V. L., Wilmouth, D. M., and Wine, P. H.: Chemical Kinetics and Photochemical Data for Use in Atmospheric Studies, Evaluation Number 18, Tech. Rep. 15, Jet Propulsion Laboratory, Pasadena, http://jpldataeval.jpl.nasa.gov, 2015.

Chin, M. and Jacob, D. J.: Anthropogenic and natural contributions to tropospheric sulfate: A global model analysis, J. Geophys. Res. Atmos., 101, 18 691–18 699, https://doi.org/10.1029/96JD01222, 1996.

Chin, M., Rood, R. B., Lin, S.-J., Müller, J.-F., and Thompson, A. M.: Atmospheric sulfur cycle simulated in the global model GOCART: Model description and global properties, J. Geophys. Res. Atmos., 105, 24 671–24 687, https://doi.org/10.1029/2000JD900384, 2000.

Ding, T., Valkiers, S., Kipphardt, H., De Bièvre, P., Taylor, P., Gonfiantini, R., and Krouse, R.: Calibrated sulfur isotope abundance ratios of three IAEA sulfur isotope reference materials and V-CDT with a reassessment of the atomic weight of sulfur, Geochim. Cosmochim. Acta, 65, 2433–2437, https://doi.org/10.1016/S0016-7037(01)00611-1, 2001.

Eriksen, T. E., Vikane, O., Swahn, C.-G., Larsson, R., Nordén, B., and Sundbom, M.: Sulfur Isotope Effects. I. The Isotopic Exchange Coefficient for the Sulfur Isotopes ^{34}S-^{32}S in the System SO_2(g)-$HSO3^-$ (aq) at 25, 35, and 45 °C., Acta Chem. Scand., 26, 573–580, https://doi.org/10.3891/acta.chem.scand.26-0573, 1972.

Fioletov, V. E., McLinden, C. A., Cede, A., Davies, J., Mihele, C., Netcheva, S., Li, S.-M., and O'Brien, J.: Sulfur dioxide (SO_2) vertical column density measurements by Pandora spectrometer over the Canadian oil sands, Atmos. Meas. Tech., 9, 2961–2976, https://doi.org/10.5194/amt-9-2961-2016, 2016.

Gerhardsson, L.: Acid precipitation-effects on trace elements and human health, Sci. Total Environ., 153, 237–245, 1994.

Ghahremaninezhad, R., Norman, A.-L., Abbatt, J. P. D., Levasseur, M., and Thomas, J. L.: Biogenic, anthropogenic and sea salt sulfate size-segregated aerosols in the Arctic summer, Atmos. Chem. Phys., 16, 5191–5202, https://doi.org/10.5194/acp-16-5191-2016, 2016.

Giesemann, A., Jaeger, H.-J., Norman, A. L., Krouse, H. R., and Brand, W. A.: Online Sulfur-Isotope Determination Using an Elemental Analyzer Coupled to a Mass Spectrometer, Anal. Chem., 66, 2816–2819, https://doi.org/10.1021/ac00090a005, 1994.

Gordon, M., Makar, P. A., Staebler, R. M., Zhang, J., Akingunola, A., Gong, W., and Li, S.-M.: A Comparison of Plume Rise Algorithms to Stack Plume Measurements in the Athabasca Oil Sands, Atmos. Chem. Phys. Discuss., pp. 1–27, https://doi.org/10.5194/acp-2017-1093, 2017.

Hains, J. C.: A chemical climatology of lower tropospheric trace gases and aerosols over themid-atlanticregion (doctoral dissertation), Ph.D. thesis, 2007.

Harris, E., Sinha, B., Hoppe, P., Crowley, J. N., Ono, S., and Foley, S.: Sulfur isotope fractionation during oxidation of sulfur dioxide : gas-phase oxidation by OH radicals and aqueous oxidation by H_2O_2, O_3 and iron catalysis, Atmos. Chem. Phys., 4, https://doi.org/10.5194/acp-12-407-2012, 2012.

Harris, E., Sinha, B., Hoppe, P., and Ono, S.: High-Precision Measurements of ^{33}S and ^{34}S Fractionation during SO_2 Oxidation Reveal Causes of Seasonality in SO_2 and Sulfate Isotopic Composition, Environ. Sci. Technol., 47, 12 174–12 183, https://doi.org/10.1021/es402824c, 2013a.

Harris, E., Sinha, B., van Pinxteren, D., Tilgner, A., Fomba, K. W., Schneider, J., Roth, A., Gnauk, T., Fahlbusch, B., Mertes, S., Lee, T., Collett, J., Foley, S., Borrmann, S., Hoppe, P., and Herrmann, H.: Enhanced Role of Transition Metal Ion Catalysis During In-Cloud Oxidation of SO_2, Science (80-.)., 340, 727–730, https://doi.org/10.1126/science.1230911, 2013b.

Hegg, D. A., Covert, D. S., Jonsson, H., Khelif, D., and Friehe, C. A.: Observations of the impact of cloud processing on aerosol light-scattering efficiency, Tellus B, 56, 285–293, 2004.

Herrmann, H., Ervens, B., Jacobi, H.-W., Wolke, R., Nowacki, P., and Zellner, R.: CAPRAM2.3: A Chemical Aqueous Phase Radical Mechanism for Tropospheric Chemistry, J. Atmos. Chem., 36, 231–284, https://doi.org/10.1023/A:1006318622743, 2000.

Hicks, B.: Dry deposition to forests—On the use of data from clearings, Agric. For. Meteorol., 136, 214–221, https://doi.org/10.1016/j.agrformet.2004.06.013, 2006.

Howell, S. G., Clarke, A. D., Freitag, S., McNaughton, C. S., Kapustin, V., Brekovskikh, V., Jimenez, J.-L., and Cubison, M. J.: An airborne assessment of atmospheric particulate emissions from the processing of Athabasca oil sands, Atmos. Chem. Phys., 14, 5073–5087, https://doi.org/10.5194/acp-14-5073-2014, 2014.

IPCC: Intergovernmental Panel on Climate Change, 2001, 2001.

Jacob, D. J. and Hoffmann, M. R.: A dynamic model for the production of H+ NO_3^-, and SO_4^{2-} in urban fog, J. Geophys. Res., 88, 6611, https://doi.org/10.1029/JC088iC11p06611, 1983.

Jacob, D. J., Waldman, J. M., Munger, J. W., and Hoffmann, M. R.: A field investigation of physical and chemical mechanisms affecting pollutant concentrations in fog droplets, Tellus B, 36B, 272–285, 1984.

Jacob, D. J., Gottlieb, E. W., and Prather, M. J.: Chemistry of a polluted cloudy boundary layer, J. Geophys. Res., 94, 12 975, https://doi.org/10.1029/JD094iD10p12975, 1989.

Kindzierski, W. B. and Ranganathan, H. K.: Indoor and outdoor SO_2 in a community near oil sand extraction and production facilities in northern Alberta, J. Environ. Eng. Sci., 5, S121–S129, https://doi.org/10.1139/s06-022, 2006.

Krouse, H. and Grinenko, V.: SCOPE 43, John Wiley & Sons, 1991.

Kulmala, M., Vehkamäki, H., Petäjä, T., Dal Maso, M., Lauri, A., Kerminen, V.-M., Birmili, W., and McMurry, P.: Formation and growth rates of ultrafine atmospheric particles: a review of observations, J. Aerosol Sci., 35, 143–176, https://doi.org/10.1016/j.jaerosci.2003.10.003, 2004.

Kulmala, M., Riipinen, I., Sipila, M., Manninen, H. E., Petaja, T., Junninen, H., Maso, M. D., Mordas, G., Mirme, A., Vana, M., Hirsikko, A., Laakso, L., Harrison, R. M., Hanson, I., Leung, C., Lehtinen, K. E. J., and Kerminen, V.-M.: Toward Direct Measurement of Atmospheric Nucleation, Science (80-.)., 318, 89–92, https://doi.org/10.1126/science.1144124, 2007.

Kumar, A., Sarin, M., and Srinivas, B.: Aerosol iron solubility over Bay of Bengal: Role of anthropogenic sources and chemical processing, Mar. Chem., 121, 167–175, https://doi.org/10.1016/j.marchem.2010.04.005, 2010.

Liggio, J., Li, S.-M., Hayden, K., Taha, Y. M., Stroud, C., Darlington, A., Drollette, B. D., Gordon, M., Lee, P., Liu, P., Leithead, A., Moussa, S. G., Wang, D., O'Brien, J., Mittermeier, R. L., Brook, J. R., Lu, G., Staebler, R. M., Han, Y., Tokarek, T. W., Osthoff, H. D., Makar, P. A., Zhang, J., L. Plata, D., and Gentner, D. R.: Oil sands operations as a large source of secondary organic aerosols, Nature, 534, 91–94, https://doi.org/10.1038/nature17646, 2016.

Lin, M., Biglari, S., and Thiemens, M. H.: Quantification of Gas-to-Particle Conversion Rates of Sulfur in the Terrestrial Atmosphere Using High-Sensitivity Measurements of Cosmogenic ^{35}S, ACS Earth Sp. Chem., 1, 324–333, https://doi.org/10.1021/acsearthspacechem.7b00047, 2017.

Mauldin III, R. L., Berndt, T., Sipilä, M., Paasonen, P., Petäjä, T., Kim, S., Kurtén, T., Stratmann, F., Kerminen, V.-M., and Kulmala, M.: A new atmospherically relevant oxidant of sulphur dioxide, Nature, 488, 193–196, https://doi.org/10.1038/nature11278, 2012.

McCabe, J. R., Savarino, J., Alexander, B., Gong, S., and Thiemens, M. H.: Isotopic constraints on non-photochemical sulfate production in the Arctic winter, Geophys. Res. Lett., 33, L05 810, https://doi.org/10.1029/2005GL025164, 2006 Isotopic, 2006.

McLinden, C. A., Fioletov, V., Boersma, K. F., Krotkov, N., Sioris, C. E., Veefkind, J. P., and Yang, K.: Air quality over the Canadian oil sands: A first assessment using satellite observations, Geophys. Res. Lett., 39, n/a–n/a, https://doi.org/10.1029/2011GL050273, 2012.

Mertes, S., Galgon, D., Schwirn, K., Nowak, A., Lehmann, K., Massling, A., Wiedensohler, A., and Wieprecht, W.: Evolution of particle concentration and size distribution observed upwind, inside and downwind hill cap clouds at connected flow conditions during FEBUKO, Atmos. Environ., 39, 4233–4245, https://doi.org/10.1016/j.atmosenv.2005.02.009, 2005a.

Mertes, S., Lehmann, K., Nowak, A., Massling, A., and Wiedensohler, A.: Link between aerosol hygroscopic growth and droplet activation observed for hill-capped clouds at connected flow conditions during FEBUKO, Atmos. Environ., 39, 4247–4256, https://doi.org/10.1016/j.atmosenv.2005.02.010, 2005b.

Myles, L., Meyers, T. P., and Robinson, L.: Relaxed eddy accumulation measurements of ammonia, nitric acid, sulfur dioxide and particulate sulfate dry deposition near Tampa, FL, USA, Environ. Res. Lett., 2, 034 004, https://doi.org/10.1088/1748-9326/2/3/034004, 2007.

Newman, L., Krouse, H. R., and Grinenko, V. A.: Sulphur isotope variations in the atmosphere, John Wiley and Sons, United Kingdom, 1991.

Norman, A.: Insights into the biogenic contribution to total sulphate in aerosol and precipitation in the Fraser Valley afforded by isotopes of sulphur and oxygen, J. Geophys. Res., 109, D05 311, https://doi.org/10.1029/2002JD003072, 2004.

Norman, A., Krouse, H., and Macleod, J.: Apportionment of Pollutants in an Urban Airshed: Calgary, Canada, A Case Study, in: Air Pollut. Model. its Appl. XVI, edited by Carlos, B. and Incecik, S., pp. 107–125, 2004.

Odame-Ankrah, C. A.: Improved Detection Instrument for Nitrogen Oxide Species, Ph.D. thesis, http://hdl.handle.net/11023/2006, 2015.

Osthoff, H. D., Odame-Ankrah, C. A., Taha, Y. M., Tokarek, T. W., Schiller, C. L., Haga, D., Jones, K., and Vingarzan, R.: Low levels of nitryl chloride: Nocturnal nitrogen oxides in the Lower Fraser Valley of British Columbia, Atmos. Chem. Phys. Discuss., 16, 1–61, https://doi.org/10.5194/acp-2017-1027, 2017.

Paul, D. and Osthoff, H. D.: Absolute Measurements of Total Peroxy Nitrate Mixing Ratios by Thermal Dissociation Blue Diode Laser Cavity Ring-Down Spectroscopy, Anal. Chem., 82, 6695–6703, https://doi.org/10.1021/ac101441z, 2010.

Percy, K. E.: Geoscience of Climate and Energy 11. Ambient Air Quality and Linkage to Ecosystems in the Athabasca Oil Sands, Alberta, Geosci. Canada, 40, 182, https://doi.org/10.12789/geocanj.2013.40.014, 2013.

Phillips-Smith, C., Jeong, C.-H., Healy, R. M., Dabek-Zlotorzynska, E., Celo, V., Brook, J. R., and Evans, G.: Sources of particulate matter components in the Athabasca oil sands region: investigation through a comparison of trace element measurement methodologies, Atmos. Chem. Phys., 17, 9435–9449, https://doi.org/10.5194/acp-17-9435-2017, 2017.

Proemse, B. C., Mayer, B., Chow, J. C., and Watson, J. G.: Isotopic characterization of nitrate, ammonium and sulfate in stack $PM_{2.5}$ emissions in the Athabasca Oil Sands Region, Alberta, Canada, Atmos. Environ., 60, 555–563, https://doi.org/10.1016/j.atmosenv.2012.06.046, 2012a.

Proemse, B. C., Mayer, B., and Fenn, M. E.: Tracing industrial sulfur contributions to atmospheric sulfate deposition in the Athabasca oil sands region, Alberta, Canada, Appl. Geochemistry, 27, 2425–2434, https://doi.org/10.1016/j.apgeochem.2012.08.006, 2012b.

Puig, R., Àvila, A., and Soler, A.: Sulphur isotopes as tracers of the influence of a coal-fired power plant on a Scots pine forest in Catalonia (NE Spain), Atmos. Environ., 42, 733–745, https://doi.org/10.1016/j.atmosenv.2007.09.059, 2008.

Sanusi, A. A., Norman, A.-l., Burridge, C., Wadleigh, M., and Tang, W.-w.: Determination of the S Isotope Composition of Methanesulfonic Acid, Anal. Chem., 78, 4964–4968, https://doi.org/10.1021/ac0600048, 2006.

Seinfeld, J. H. and Pandis, S. N.: Atmospheric Chemistry and Physics: From Air Pollution to Climate Change, Wiley and Sons, New York, USA, 1998.

Simpson, I. J., Blake, N. J., Barletta, B., Diskin, G. S., Fuelberg, H. E., Gorham, K., Huey, L. G., Meinardi, S., Rowland, F. S., Vay, S. A., Weinheimer, A. J., Yang, M., and Blake, D. R.: Characterization of trace gases measured over alberta oil sands mining operations: 76 speciated C_2-C_{10} volatile organic compounds (VOCs), CO_2, CH_4, CO, NO, NO_2, NO_y, O_3 and SO_2, Atmos. Chem. Phys., 10, 11 931–11 954, https://doi.org/10.5194/acp-10-11931-2010, 2010.

Sipilä, M., Jokinen, T., Berndt, T., Richters, S., Makkonen, R., Donahue, N. M., Mauldin III, R. L., Kurtén, T., Paasonen, P., Sarnela, N., Ehn, M., Junninen, H., Rissanen, M. P., Thornton, J., Stratmann, F., Herrmann, H., Worsnop, D. R., Kulmala, M., Kerminen, V.-M., and Petäjä, T.: Reactivity of stabilized Criegee intermediates (sCIs) from isoprene and monoterpene ozonolysis toward SO_2 and organic acids, Atmos. Chem. Phys., 14, 12 143–12 153, https://doi.org/10.5194/acp-14-12143-2014, 2014.

Sjostedt, S., Huey, L., Tanner, D., Peischl, J., Chen, G., Dibb, J., Lefer, B., Hutterli, M., Beyersdorf, A., Blake, N., Blake, D., Sueper, D., Ryerson, T., Burkhart, J., and Stohl, A.: Observations of hydroxyl and the sum of peroxy radicals at Summit, Greenland during summer 2003, Atmos. Environ., 41, 5122–5137, https://doi.org/10.1016/j.atmosenv.2006.06.065, 2007.

Soares, J., Makar, P. A., Aklilu, Y.-a., and Akingunola, A.: Associativity Analysis of SO_2 and NO_2 for Alberta Monitoring Data Using KZ Filtering and Hierarchical Clustering, Atmos. Chem. Phys. Discuss., pp. 1–31, https://doi.org/10.5194/acp-2017-1126, 2018.

Sofen, E. D., Alexander, B., and Kunasek, S. A.: The impact of anthropogenic emissions on atmospheric sulfate production pathways, oxidants, and ice core $\Delta^{17}O(SO_4^{2-})$, Atmos. Chem. Phys., 11, 3565–3578, https://doi.org/10.5194/acp-11-3565-2011, 2011.

Tanaka, N., Rye, D. M., Xiao, Y., and Lasaga, A. C.: Use of stable sulfur isotope systematics for evaluating oxidation reaction pathways and in-cloud-scavenging of sulfur dioxide in the atmosphere, Geophys. Res. Lett., 21, 1519–1522, https://doi.org/10.1029/94GL00893, 1994.

Tokarek, T. W., Brownsey, D. K., Jordan, N., Garner, N. M., Ye, C. Z., Assad, F. V., Peace, A., Schiller, C. L., Mason, R. H., Vingarzan, R., and Osthoff, H. D.: Biogenic Emissions and Nocturnal Ozone Depletion Events at the Amphitrite Point Observatory on Vancouver Island, Atmosphere-Ocean, 55, 121–132, https://doi.org/10.1080/07055900.2017.1306687, 2017.

Twomey, S.: Aerosols, clouds and radiation, Atmos. Environ. Part A. Gen. Top., 25, 2435–2442, https://doi.org/10.1016/0960-1686(91)90159-5, 1991.

Wadleigh, M. and Blake, D.: Tracing sources of atmospheric sulphur using epiphytic lichens, Environ. Pollut., 106, 265–271, https://doi.org/10.1016/S0269-7491(99)00114-1, 1999.

Welz, O., Savee, J. D., Osborn, D. L., Vasu, S. S., Percival, C. J., Shallcross, D. E., and Taatjes, C. A.: Direct Kinetic Measurements of Criegee Intermediate (CH_2OO) Formed by Reaction of CH_2I with O_2, Science (80-.)., 335, 204–207, https://doi.org/10.1126/science.1213229, 2012.

Yuskiewicz, B. A., Stratmann, F., Birmili, W., Wiedensohler, A., Swietlicki, E., Berg, O., and Zhou, J.: The effects of in-cloud mass production on atmospheric light scatter, Atmos. Res., 50, 265–288, https://doi.org/10.1016/S0169-8095(98)00107-0, 1999.